USING DEM TO INVESTIGATE BOUNDARY CONDITIONS FOR ROCKING URM FAÇADES SUBJECTED TO EARTHQUAKE MOTION

FRANCISCO GALVEZ[1*], LUIGI SORRENTINO[2], DMYTRO DIZHUR[3] AND JASON M. INGHAM[4]

[1]PhD candidate. University of Auckland, Civil and Environmental Engineering Department, Newmarket Campus, 314-390 Khyber Pass Road, Auckland 1023, Aotearoa New Zealand
email: fglv390@aucklanduni.ac.nz, (*corresponding author)

[2] Associate Professor. Sapienza Università di Roma,
Department of Structural and Geotechnical Engineering, Faculty of Architecture,
via Antonio Gramsci 53, 00197 Roma, Italy
email: luigi.sorrentino@uniroma1.it

[3]Associate Professor. University of Auckland, Civil and Environmental Engineering Department, Newmarket Campus, 314-390 Khyber Pass Road, Auckland 1023, Aotearoa New Zealand
email: ddiz001@aucklanduni.ac.nz

[4]Professor. University of Auckland, Civil and Environmental Engineering Department, Newmarket Campus, 314-390 Khyber Pass Road, Auckland 1023, Aotearoa New Zealand
email: j.ingham@auckland.ac.nz

Abstract: *Façade overturning is a frequently observed collapse mechanism occurring in unreinforced masonry (URM) buildings during high-intensity earthquake-induced shaking. Following complete separation from a building, the rocking motion of a URM façade and the associated impact against the return walls are the factors that continue to contribute to the façade out-of-plane capacity. Seismic vulnerability studies of URM façades have historically neglected the interaction between building earthquake response and the rocking response of the façade, whereas in the study reported herein this interaction was analysed using the discrete element modelling (DEM) approach, resulting in a façade out-of-plane capacity reduction. The increment in the dynamic rocking capacity caused by the frictional connection between the URM façade and the building was also analysed and is reported.*

Keywords: Rocking Façade, Unreinforced Masonry, Boundary Conditions, Incremental Dynamic Analysis, Discrete Element Method

1. INTRODUCTION

Façade overturning is a collapse mechanism that is routinely observed after high-intensity earthquakes (Lagomarsino, 1998, Benito et al., 2007, Hess, 2007, Dizhur et al., 2010), being a critical life-safety hazard because out-of-plane failure can jeopardise the gravity-load bearing capacity of the building (Bruneau, 1994) and can result in large quantities of masonry debris falling outside the building footprint (Abeling and Ingham, 2020). Therefore, details of the collapse behaviour of unreinforced masonry (URM) façades need to be well understood. Façades that lose their connection with the adjoining return walls have been observed to behave as rocking rigid-bodies when disintegration of the masonry did not occur (Shawa et al., 2012, Lagomarsino, 2015, Giresini et al., 2018). Amongst the different approaches adopted to simulate the free rocking behaviour of rigid bodies, the strategy originally developed by Housner (1963) is the most widely used where the rocking equations of motion represent a rigid block rocking on a simply supported rigid base, with the assumption that the coefficient of friction is large enough to avoid sliding. The cyclic rocking motion of a block dissipates energy when impacting the ground, which was modelled by Housner (1963) using the coefficient of restitution, such that a reduction of angular velocity occurs by assuming the conservation of angular momentum before and after every impact. Several authors have revisited the Housner (1963) formulation to include sliding and bouncing in the rocking motion (Aslam et al., 1975, Ishiyama, 1982, Psycharis and Jennings, 1983), to account for different material stiffnesses and different friction characteristics at the block-base contact (ElGawady et al., 2011, Lipo and de Felice, 2016, Ther and Kollár, 2016), to reduce discrepancies with experimental observations (Lipscombe and Pellegrino, 1993, Kalliontzis et al., 2016), or to reduce the complexity of the rocking motion formulation in order to facilitate the development of a closed-form solution to the problem (Casapulla and Maione, 2017).

The abovementioned research gives a solution to the problem of a free-standing rocking block, but many rocking elements that concern the earthquake engineering community are one-sided rocking blocks (e.g. hospital or laboratory equipment generally placed next to walls, or rocking unreinforced masonry such as URM façades). The motion of the façades when constrained by impacting with the return walls makes the problem significantly more complex, and therefore less research has been conducted on this topic. Impact interaction has been accounted for by restricting the cyclic motion and including an extra coefficient of restitution that changes the amplitude and the sign of the rotational velocity instantaneously to account for the change in motion direction and the energy dissipated at the contact (Sorrentino et al., 2008, Bao and Konstantinidis, 2020). Another adopted approach was to assume that the energy dissipated between the rocking blocks and the adjacent walls was negligible (Sigurdsson et al., 2019).

One-sided rocking models that account for interaction between the rocking façade and steel tie rods were also reported (Giresini et al., 2015, Giresini and Sassu, 2016, Giresini, 2017, AlShawa et al., 2019) and simplified approaches were proposed where the interaction between façades and return walls was represented by a bed of springs (Giresini and Sassu, 2016, Giresini, 2017). Using the same modelling strategy, more recent models have included two-directional motion of more complex masonry shapes (e.g. corner failure macroblock) (Casapulla et al., 2019a, Giresini et al., 2019). Researchers agree that the overturning frequency of façades is reduced when the damping associated with impact with the return wall is increased (Sorrentino et al., 2008, Sorrentino et al., 2011, Bao and Konstantinidis, 2020), and when steel ties are used as a strengthening solution (Giresini, 2017, AlShawa et al., 2019). Bao and Konstantinidis (2020) considered a sliding-rocking block adjacent to a wall and concluded that decreasing the friction coefficient and reducing the gap between block and wall are beneficial strategies to increase the dynamic stability against overturning while accepting sliding. Casapulla et al. (2017) provides a detailed review of the latest advances on rocking and kinematic analysis of URM walls subjected to earthquakes.

Façades that span over several stories and where the parapet is located at the top of the URM building experience distinctly different earthquake motion than that occurring at ground level, because earthquake motion at the ground surface is modified and amplified as it travels through the structural elements of the building. This amplification phenomenon is acknowledged and well documented in the literature (Priestley, 1985, Derakhshan et al., 2014, Degli Abbati et al., 2018) when assessing the seismic performance of URM parapets or upper level URM walls. The inelastic behaviour of the building also modifies the ground motion up the building height, dissipating energy as building damage occurs. Depending on the ductility and the stiffness of the building, the modification of the ground motion may be either beneficial or detrimental to the seismic demand of the upper level walls (Menon and Magenes, 2011). However in the case of URM façades, studies generally do not account for different input motions at the base and up the height of the return walls (Sorrentino et al., 2008, Shawa et al., 2012, Giresini et al., 2019, Sigurdsson et al., 2019). In the study presented herein four topics are addressed using the discrete element method (DEM): (1) finding a simple alternative to model the amplification of ground motion occurring in URM buildings, (2) developing and experimentally validating a suitable strategy to assign a damping parameter for one-sided rocking façades, (3) studying the seismic vulnerability of URM façades with different boundary conditions, and (4) analysing the influence when including the seismic behaviour of the building during an assessment of the vulnerability of rocking façades. Ideally, either the complete building or alternatively part of the building would be micro-modelled and analysed with thousands of degrees of freedom (DOF), but such an approach is computationally demanding making such an undertaking impractical. Instead, an alternative method was investigated and the seismic response for various configurations of lumped mass-spring models were compared. Once the simpler model configuration was selected, the resulting motion at multiple levels within the building was extracted and used as input to the simulated return walls of an experimentally validated 3D DEM simulation of rocking façades spanning over two building storeys.

2. COMPARISON BETWEEN LUMPED MASS-SPRING AND 3D DEM MODELS

A single-unit two-storey URM case study building that was used in the Italian ReLUIS III research Project *Masonry Structures* was selected in order to study the modification of ground motion occurring up the height of a URM building. The selected building was designed with a relatively simple geometry that was intended to reveal interaction effects between piers and spandrels. The geometry of the case study building also facilitated a study of the effects of stress redistribution in the presence of walls with different stiffness, plus a study of torsional effects. This building was extensively studied by others previously using a multitude of modelling techniques (Cattari et al., 2018, Olcese, 2018). As part of the study reported herein, the geometry of the building was modelled using the software Rhinoceros® (McNeel and Associates, 2014), which allows a script to be run that contains an algorithm capable of exporting a text file of the building geometry compatible with the DEM software 3DEC (Itasca, 2013) (see Figure 1).

(a) Rhinoceros® (Dimensions in m) (b) DEM

Figure 1: Geometrical model of the two-storey case study building

The DEM software allows modelling of every masonry unit by independent rigid or deformable elements connected to each other by nonlinear interfaces. The case study building presented herein was modelled with rigid elements referred to herein as bricks, and linearly elastic interfaces. This linear behaviour complies with the assumption that façades and parapets will collapse before the building has suffered enough damage to alter its fundamental frequency, that will allow a simplification of the problem to focus on the façade boundary condition problem addressed herein. Rigid diaphragms with elastic connections were modelled as per Gubana and Melotto (2019). The diaphragm comprised evenly spaced rigid beams oriented parallel to the shorter walls and placed on top of the masonry walls, whose thickness was reduced to host the beam support. Elastic contacts between the beam ends and the masonry were generated and in order to simulate actual diaphragms, a rigid panel was modelled on top of the beams and connected to them with elastic contacts. This simplified modelling strategy allowed the cyclic behaviour of a timber floor to be considered in the DEM model.

The interfaces between the bricks were defined by three shear and normal material parameters: normal stiffness (j_{kn}); shear stiffness (j_{ks}); friction angle (˚). Generally, the estimation of j_{kn} is calculated as E/s, where E is the Young modulus and s is the joint spacing (see Galvez et al. (2018) for further details). The value of E for the case study building was 1,800 MPa, and the dimensions of the bricks were 24L × 6H × 12W cm^3. However, application of these parameters to forecast j_{kn} led to an overestimation of the overall stiffness of the building and a much lower fundamental period than is typical for a 2-storey URM building. Hence it was decided to reduce j_{kn} until the building modes of vibrations resulted in values that were similar to previous observations but respected the relationship with brick dimensions. This tuning strategy to establish the material properties has been implemented by multiple researchers (Papantonopoulos et al., 2002, Psycharis et al., 2003, Lemos and Campos Costa, 2017, Meriggi et al., 2019) who calibrated their models by best fitting stiffness parameters to match experimental dynamic behaviour or by replicating previous similar research. There are three types of contact surfaces around a brick, each with its own properties influenced by the brick dimensions: head joint (j_{kn} = 1,280 MPa/m, j_{ks} = 422 MPa/m, friction angle = 30°), bed joint (j_{kn} = 5,120 MPa/m, j_{ks} = 1,690 MPa/m, friction angle = 30°) and collar joint (j_{kn} = 2,560 MPa/m, j_{ks} =845 MPa/m, friction angle = 30°). The aforementioned joint material properties were selected to ensure that the eigenvalue analysis delivered a period of 0.25 s for the Y translational mode of vibration, coinciding with the estimate given by equation $T = 0.0625 \cdot h^{0.75}$ from NZS1170.5 (2004) and AS1170.4 (2007). The same analysis delivered a period of 0.16 s for the Z rotational mode (see Figure 2). To these frequencies 5% and 3% Rayleigh mass proportional (MP) damping ratios were applied, respectively. Rayleigh damping can be derived using MP or stiffness proportional (SP) damping, with the latter having a strong influence on the timestep size of the simulation. A time-history simulation of the complete building using DEM (CBDEM) was considered highly computationally demanding even when using MP damping. Consequently a simplified structure (SBDEM) without the front and rear façades in the direction of motion, *Y*, was dynamically compared to the complete building model via eigenvalue analysis (see Figure 2).

(a) 1st mode of CBDEM (T=0.25 s) | (b) 1st mode of SBDEM (T=0.27 s) | (c) 2nd mode of CBDEM (T=0.16 s) | (d) 2nd mode of SBDEM (T=0.17 s)

Figure 2: First and second modal shapes and periods in the *Y* direction of the complete and the simplified structure calculated using DEM modal analysis

Considering the directionality of the input motion, only the modes of vibration with significant effective modal mass in the *Y* axis were considered, with a difference of 0.01-0.02 s between the modal frequencies and similar deformed shapes being observed in Figure 2. Subjecting even the SBDEM building to multiple time-history analyses would require a great computational effort and would highly restrict the number of earthquakes that could be amplified as input to the rocking façade simulations. Hence, developing a simpler easy-to-run equivalent model had a high potential for future studies. The simpler model chosen to compute the dynamic behaviour of the building was based on the solution of the explicit formulation of the equation of motion of a spring-mass model with translational degrees of freedom and varying number of springs and lumped masses (SMDOF) performed in the software Matlab® (MathWorks, 2008). All the masses of the model were divided equally per lumped mass, and the summation of all mass was equal to the mass of the SBDEM model. Similarly, all the stiffnesses were equal and adjusted so that the first mode of vibration matched the value of 0.27 s that was obtained from the SBDEM model (Figure 2b), while damping was fixed at 5%. After confirming the directional dynamic equivalence between the CBDEM and the SBDEM (see Figure 2), the seismic response of the SBDEM when subjected to two of the ground motions in Table 1 (BUCAR0 and RRS228) was compared to the response of the SMDOF.

(a) Time-history response

(b) Response Spectra

(c) Power Spectra

Figure 3: Comparison between the seismic response of the SBDEM and SMDOF for BUCAR0 earthquake.

The SMDOF model that provided results most similar to the results from the SBDEM was identified by comparing the weighted mean error (WME) between models using SBDEM as the reference. The WME was obtained from the time-history responses and the acceleration and power spectra (see Figure 3) with the following formulation:

$$\mathrm{WME} = \frac{\int_0^X \mid Y_{DEM}(x) - Y_{DOF}(x) \mid dx}{\int_0^X \mid Y_{DEM}(x) \mid dx} \tag{1}$$

where x was time, period or frequency, Y was acceleration, spectral acceleration or power amplitude depending on the evaluated case and X was the total range of x considered. Observing Table 2, the errors generated for a 4DOF and 5DOF models were found to have minimal difference. Consequently a 4DOF substitute structure was chosen to obtain the motion to apply to the rocking parapets and façade. A 4DOF model is more efficient than a 2DOF with masses lumped at floors, because most of the mass of typical masonry buildings is located in the walls rather than in the diaphragms. It was assumed that the primary building structure did not suffer damage during the earthquake and that even if damage appeared, the parapet and façade would collapse before the building sustained sufficient damage to change the stiffness and therefore the response. DEM simulations are known to have high-frequency numerical noise in the solution, known as the “rattling effect” (Lorig and Hart, 1993, Papantonopoulos et al., 2002, Jing and Stephansson, 2007, Dimitri et al., 2011). Because of the high-frequency nature of this effect, MP damping is unable to attenuate this effect, which can affect the simulation depending on the magnitude of the frequencies of phenomena to be modelled. The rattling effect for the SBDEM can be observed from 0 to 1 s of the response in Figure 3a and in the peak around 0.08 s of the spectra in Figure 3c. In this problem, the rattling error did not affect the main response of the building, which was approximately 0.27 s.

3. VALIDATION OF DAMPING PARAMETERS FOR ROCKING FAÇADES

Rayleigh damping makes use of the constants α (MP) and β (SP) to construct the damping matrix when performing dynamic analysis. The relationship for the damping ratio (ζ_n) for any circular frequency (ω_n) that results from the application of α and β can be found in Bathe and Wilson (1976) as:

$$\zeta_n = \frac{\alpha}{2 \cdot \omega_n} + \frac{\beta \cdot \omega_n}{2} \tag{2}$$

Rocking simulations using SP damping have been recommended by several authors (DeJong, 2009, Tomassetti et al., 2019) because MP damping may introduce overdamped low frequencies and result in unrealistic results. However, a systematic approach has not yet been developed to assign the value of SP damping for a 1SR wall. Conversely, a formulation experimentally developed by Sorrentino et al. (2011) allowed for an estimation of the restitution coefficient ($e_{1\mathrm{SR}}$) caused by multiple impacts of the block into the return walls as:

$$e_{1\mathrm{SR}} = \left(1 - \frac{3}{2}\cdot\sin^2\alpha\right)^2 \cdot \left(1 - \frac{3}{2}\cdot\cos^2\alpha\right) \tag{3}$$

A parametric analysis was performed using single DEM blocks to represent the cracked rocking façade and interaction with the return walls to investigate β for 1SR ($\beta_{1\mathrm{SR}}$) walls based on their equivalent $e_{1\mathrm{SR}}$. The j_{kn} at the bottom of the walls was calculated as E/h, where h is the height, and j_{kn} for the joint interacting with the return walls was calculated as E/L, where L is the average length of the triangular-shaped URM block assumed to develop in the return wall once cracking occurs at 45°, according to the observations of Giresini and Sassu (2016). Assigning the value of j_{kn} for the return wall is a challenging task with various limitations as outlined by Giresini (2017). First, it is common practice to assume that the stiffness of the return walls is constant, even though it is known that the seismic response of URM buildings is characterised by progressive damage, and the corresponding change in stiffness can have an influence on the out-of-plane response of URM walls (Menon and Magenes, 2011). Secondly, the cracks on the return walls are assumed to occur at 45° even though the crack angle is actually unknown.

Four batches of simulations having varying block geometry [height (h) and thickness (b)] and varying stiffness of the interface between the returning walls and the façade were performed and the results are summarised in Figure 4. The façade was displaced from the return walls, released, and allowed to rock and impact against the return walls. A range of $\beta_{1\mathrm{SR}}$ parameters was applied to the walls where the first three bounces after impacting with the return walls were studied based on the observations of Sorrentino et al. (2011), who found that the experimental coefficient of restitution of the third impact calculated using the Housner (1963) formulation was generally the closest to $e_{1\mathrm{SR}}$. The formulation for the experimental coefficient can be seen in equation 4, where $|\theta_n|$ is the maximum absolute rotation at the n^{th} impact and $\eta = tan^{-1}\left({}^{b}/_{h}\right)$.

$$e_{exp} = \sqrt[2n]{\frac{1-\left(1-\frac{|\theta_n|}{\eta}\right)^2}{1-\left(1-\frac{|\theta_0|}{\eta}\right)^2}} \tag{4}$$

Figure 4a shows the values of β_{1SR} used as part of the parametric study for various values of h and a constant value of b = 0.11 m. The values to parametrise β_{1SR} were chosen ranging from a maximum expected for a single rocking block as derived from DeJong (2009) and a minimum obtained for two blocks vertically stacked obtained using the same principles as DeJong (2009) recommended. Assuming from Sorrentino et al. (2011) that e_{exp} is between 64% and 72% of e_{1SR} on the first impact, between 74% and 86% on the second impact, and that on the third impact eexp is similar to e_{1SR}, the best fitting free rocking results of DEM simulations using β_{1SR} are highlighted in Figure 4a. To calculate the best fitting results, e_{exp} (Equation 4) was computed from the results of the DEM simulations and compared to the aforementioned percentages of e_{1SR} (Equation 3) on the first, second and third bounce. The best fitting trends for different h/b of façades with b = 0.11, 0.3 m and E = 1800, 4050 MPa, as observed in Figure 4b, where studied to obtain a dimensional regression for estimating β_{1SR} as follows:

$$\beta_{1SR} = \left(\frac{b}{384} - \frac{E}{5.6\times10^6} + 0.00074\right)\cdot e^{\left({}^{h}/_{b}\cdot\frac{-E+6572}{1.2\times10^5}\right)} \tag{5}$$

wherein b has units of m, and E of MPa.

(a) Values of β_{1SR} for walls with b = 0.11 m, E = 1800 MPa and different values of h/b.

(b) Best fitting β_{1SR} for different values of E and geometry variations

Figure 4: Parametric studies.

The experimental setup reported by Sorrentino et al. (2011) and by Shawa et al. (2012) were used to validate the predictions made using equation 5. Sorrentino et al. (2011) tested a wall of 0.8 m height, 0.11 m thickness, E = 1800 MPa and density = 1750 kg/m^3 built with solid clay bricks together with two return walls disconnected with a dry joint (see Figure 5a). The tested wall was displaced from the return walls, released and allowed to rock in order to study the attenuation caused by the impacts against the return walls. Observing the time-history plots in Figure 5b,c, the simulation performed using β_{1SR} = 0.00025 was found to be closest to the experiments during the first bounce, but from the values of e_{exp} plotted in Figure 5d the simulation with β_{1SR} = 0.001 showed similar damped motion as the experiments during the second and third bounces. The value of β_{1SR} obtained using equation 5 was 0.00095, which was deemed an acceptable result for being only 5% different from β_{1SR} = 0.001. After the first bounce of simulations with β_{1SR} = 0.000125, 0.00025, 0.0005 and 0.001 the majority of the energy was dissipated and the second and third bounces remained mostly undamped. Alternatively, simulations with β_{1SR} = 0.002, 0.004 and 0.0058 were found to be overdamped after the first impact.

(a) Experimental setup (Sorrentino et al., 2011)

(b) Complete time-history

(c) Expanded view between 0.9 s and 1.9 s

(d) Values of e_{exp} for different simulations using β_{1SR} compared to e_{1SR} and experimental testing

Figure 5: Experimental testing from Sorrentino et al. (2011) and simulations using 3DEC

Shawa et al. (2012) subjected a 3 m high and 0.25 m thick tuff masonry wall to four earthquakes named BagnirWE, SturWE, R1168EW and CalitWE (more information can be found in Shawa et al. (2012)). The wall was constructed with return walls to perform 1SR and a physical gap of 4 mm was reported between the return walls and the overturning wall. During repeated rocking testing debris accumulated under the wall and prevented the wall from returning to its initial vertical position, such that on repeated shaking the wall had rotated (φ) initial geometry. The shake table experimental campaign performed by Shawa et al. (2012) was simulated using SP damping and the reported material properties of E = 4050 MPa (j_{kn} = 1350 MPa/m) and density=1810 kg/m^3, with care taken to account for the reported geometrical irregularities due to debris lodged beneath the wall (Figure 6a,b). It is worth noting that Shawa et al. (2012) was capable of reproducing the 1SR tests with a model based on Housner (1963) approach taking into account the multiple impacts energy dissipation for the coefficient of restitution and with a 2D DEM model with SP damping. Applying equation 5, $\beta_{1\mathrm{SR}}$ was found to be 0.00086, a very similar value as the one found by trial and error by Shawa et al. (2012) ($\beta_{1\mathrm{SR}}$ = 0.00094) for a test of the early stages of the testing sequence. In later stages the value of damping increased as a consequence of damage due to mortar deterioration and cracking due to the impact with the return walls (Shawa et al., 2012). Using equation 5 as a starting point for the assignation of $\beta_{1\mathrm{SR}}$, the damping value was slowly increased until reaching a good agreement between experimental observations and 3D DEM as seen in Figure 6. When simulating the four earthquakes Shawa et al. (2012) found similar values for $\beta_{1\mathrm{SR}}$. Although equation 5 appears to deliver reasonable estimation of $\beta_{1\mathrm{SR}}$, additional research is required to achieve a robust criterion for selection of a damping value that accounts for diffenre boundary conditions including free-standing blocks.

(a) DEM model

(b) Diagram of tilted rocking facade

(c) BagnirWE, $\varphi = 0.191°$

(d) SturWE, $\varphi = 0.210°$

(e) R1168EW, $\varphi = 0.272°$

(f) CalitWE, $\varphi = 0.348°$

Figure 6: Comparison of top displacement between experiments and DEM simulation.

4. DIFFERENT BOUNDARY CONDITIONS FOR ROCKING FAÇADES

The rocking interaction between the façade (dimensions in Figure 1a) and the case study URM building was simulated using three structural configurations and two variations in material characteristics to arrive at five different boundary condition scenarios that utilised springs (see Figure 7) calibrated to replicate the deformation of the return wall. First, each return wall was modelled using a single cohesionless block behind the façade and subjected to the same ground motion as at the façade base (W1, see Figure 7a). Secondly, each return wall was modelled using four cohesionless blocks positioned at the back of the façade, with the ground motion applied to the base and with the amplified motions extracted from each lumped mass of the 4DOF model being input to each block positioned above the base (W2, see Figure 7b). Considering the minimal differences between 4DOF and 5DOF models (Table 2), the use of the former model was considered adequate. The aforementioned models were also simulated with 0.1 MPa cohesion and 0.07 MPa tensile strength (Giaretton et al., 2016) on the contact interface between the façade and the return walls. Finally, a more detailed model that accounted for friction (friction angle = 30 $^\circ$) with no cohesion between the façade and the return walls, and including the 4DOF amplified motions, was modelled (W3, see Figure 7c). All façade configurations were modelled using a value of β_{1SR} = 0.00276 according to equation 5.

(a) W1 (b) W2 (c) W3

Figure 7: DEM modelling of rocking façade and return walls with associated block and spring interaction scheme (Colours represent displacement magnitude without scale).

Elements representing connection between the façade and the return walls in W3 were carefully modelled to avoid increments in the overturning resistance being in excess of a realistic contribution of masonry interlocking. There were two crucial phenomena to keep in mind while assigning the degrees of freedom to the return wall bricks: (1) friction forces resulting on the brick interfaces are proportional to the weight from the upper bricks while the façade is rotating with respect to the return wall, (2) the interlocked bricks of the return walls need to rotate in opposite directions to form the crack between the façade and return walls (see Figure 8b). Therefore, during the induced motion each brick in the return wall (Figure 8a) had free translational movement in the *Z* (vertical) direction and free rotation around the *X* axis, while having the remaining degrees of freedom restricted and being capable of moving horizontally with the amplified input motion. Low values of the normal and shear stiffnesses of the connection between the façade and the return walls were chosen in order to reduce computational time (j_{kn} = 1,100 MPa/m and j_{ks} = 440 MPa/m). These values did not influence the final capacity of the wall but only the stiffness of the connection (Mordanova et al., 2017, Pulatsu et al., 2020), which was suitable for this study. Due to the rigidity of the façade and return wall elements, the lower wall courses remained connected by their edges when the rotation was well advanced, resulting in a non-realistic resistance. For this reason, lower elements of the return walls were modelled with an inclined interface to allow breaking in shear (see lower courses of Figure 8a). The partial elements from the façade (see Figure 8a) were connected using an interface with appropriate material properties for fired clay bricks to allow for deformation and detachment if needed. In order to reduce the computation time, the least possible number of elements were included by modelling only one column of return wall bricks, and by increasing and modifying the dimensions of the bricks compared to what are usually used in construction (0.25L × 0.324H × 0.375W m^3). Prior to running the dynamic simulation a pushover test was performed to confirm that the boundary conditions were realistically modelled. Figure 8c shows good agreement between kinematic capacity curves developed by Casapulla et al. (2019b) and the DEM simulation.

(a) Elements in W3

(b) Scheme of generic façade and return wall separation

(c) Comparison between kinematic and DEM capacity curve

Figure 8: W3 details and capacity curve

The five different models shown in Figure 7 were subjected to the four earthquakes presented in Table 1 in the positive (+) and negative (-) directions, with increasing acceleration. The dynamic capacity curve of each wall configuration in terms of PGA and maximum top displacement (*d*) of the façade was normalized by the wall width (*w*) and is plotted in Figure 9, showing that W2 tended to be equally vulnerable or more vulnerable than W1. Though by a very small margin, for BUCAR0-, BUCAR0+, 1ST280-, HVSC1+ and RRS228+ the dynamic behaviour of the building caused a slightly more vulnerable capacity for W2. Conversely, the dynamic amplification of the building caused a marked reduction in façade capacity for the remainder of the cases. When cohesion was added to the W1 model a clear increment in resisting acceleration was observed, while when cohesion was included in the W2 wall the motion of the return walls made the rigid façade detach at an early stage, resulting in premature collapse. The dynamic incremental capacity curve of W3 highlights the importance of interlocking on out-of-plane response. BUCAR0 and RRS228 records both feature a large pulse and resulted in IDA curves that matched well with the pushover curve obtained via quasi static analysis undertaken by Casapulla et al. (2019b). The results from 1ST280 and HVSC1 showed that the capacity of rocking blocks when subjected to earthquakes can be much higher than obtained from equivalent-static pushover.

BUCAR0

RRS228

1ST280

HVSC1

Figure 9: Incremental dynamic analyses (Positive (+) direction – Left; Negative (-) direction – Right. Pushover curves in grey for reference).

5. CONCLUSIONS

Nonlinear incremental dynamic analyses were performed using the three dimensional discrete element method to investigate the vulnerability of a rocking façade as part of a two-storey case study unreinforced masonry building. Due to computational restrictions and simulation time practicality, dynamically equivalent strategies were developed to simulate the building behaviour associated with amplification of the ground motion and interaction between the rocking façade and the return walls. The adopted strategy consisted of developing a 4 degrees of freedom spring-mass model of the two-storey unreinforced masonry building that was used to efficiently simulate several time-history analyses and obtain the amplified motion. The amplified motion of each lumped mass was applied to a discrete element method model of the rocking façade with different boundary conditions. The equivalence between a full-scale 3D discrete element method discretised model and the 4 degrees of freedom substitute structure was demonstrated by subjecting both models to earthquake ground motions and comparing the time history performance of the building motion, the spectral acceleration and the frequency power spectra.

In order to assure that the rocking simulations of facades using discrete element method were performed accurately, a formulation was developed to assign an appropriate value of damping following a stiffness proportional damping approach. The capability of the developed formulation to be used for any façade independent of the geometry and material properties was validated using experimental free rocking and earthquake shake-table testing.

Comparisons of the incremental dynamic capacity curves showed that modelling the behaviour of the building, as opposed to the usual strategy of having non-amplified excitation of the return walls, can reduce the capacity of the façade by as much as 60% depending on the characteristics of the earthquake. This observation implies that when nonlinear time-history analyses are used to assess the overturning vulnerability of one-sided rocking parts, the capacity of such elements may be overestimated. Furthermore, applying amplified motion to return walls having cohesive bond resulted in premature collapse of the façade such that this strategy is not advised to be used in future studies. On the contrary, detailed modelling of the interlocking elements of the façade with the return walls that were subjected to amplified motion was found to considerably increase the capacity of the façades, depicting greater capacity than shown via the pushover analysis. While the capacity value will change depending on the level of connectivity between the return walls and the façade, the increment in capacity due to rocking behaviour will remain. Lower bricks of the return walls in the detailed model were designed specifically for the problem studied herein. Further research of the rocking problem is required to address stress concentration occurring in lower rigid elements due to the overturning moment, because this concentration could lead to an overestimation of the rocking capacity.

Data Availability Statement. Some or all data, models, or code that support the findings of this study are available from the corresponding author upon reasonable request.

Acknowledgements. This project was (partially) supported by QuakeCoRE, a New Zealand Tertiary Education Commission-funded Centre. This is QuakeCoRE publication number 634. The authors also gratefully acknowledge the software 3DEC provided by Itasca consulting group under the Itasca Educational Partnership program. Use was made in this paper of a solid geometry generation tool developed by Dr. Daniele Malomo, (MDRG-Matthew DeJong Research Group, University of California, Berkeley), who is gratefully acknowledged.

REFERENCES

Abeling, S. and J. M. Ingham (2020). "Volume loss fatality model for as-built and retrofitted clay brick unreinforced masonry buildings damaged in the 2010/11 Canterbury earthquakes." Structures **24**: 940-954.

AlShawa, O., D. Liberatore and L. Sorrentino (2019). "Dynamic One-Sided Out-Of-Plane Behavior of Unreinforced-Masonry Wall Restrained by Elasto-Plastic Tie-Rods." International Journal of Architectural Heritage **13**(3): 340-357.

AS1170.4 (2007). Structural design actions, Part 4: Earthquake actions in Australia. , Standards Australia.,

Aslam, M., W. G. Godden and D. T. Scalise (1975). Sliding Response of Rigid Bodies to Earthquake Motions. A Report of an Analytical and Experimental Study of the Sliding Response of Rigid Blocks Under Simultaneous Hori zontal and Vertical Earthquake Accelerations. Contract No. W-7405-eng-48. U. S. E. R. a. D. Administration., Bao, Y. and D. Konstantinidis (2020). "Dynamics of a sliding- rocking block considering impact with an adjacent wall." Earthquake Engineering & Structural Dynamics **49**(5): 498-523.

Bathe, K. J. and E. L. Wilson (1976). Numerical methods in finite element analysis. NJ, Prentice-Hall.

Benito, B., R. Capote, P. Murphy, J. M. Gaspar-Escribano, J. J. Martinez-Diaz, M. Tsige, D. Stich, J. Garcia-Mayordomo, M. J. Garcia Rodriguez, M. E. Jimenez, J. M. Insua-Arevalo, J. A. Alvarez-Gomez and C. Canora (2007). "An Overview of the Damaging and Low Magnitude Mw 4.8 La Paca Earthquake on 29 January 2005: Context, Seismotectonics, and Seismic Risk Implications for Southeast Spain." Bulletin of the Seismological Society of America **97**(3): 671-690.

Bruneau, M. (1994). "State-of-the-Art Report on Seismic Performance of Unreinforced Masonry Buildings." Journal of Structural Engineering, **120**(1): 230-251.

Casapulla, C., L. Giresini, L. U. Argiento and A. Maione (2019a). "Nonlinear Static and Dynamic Analysis of Rocking Masonry Corners Using Rigid Macro-Block Modeling." International Journal of Structural Stability and Dynamics, 10.1142/s0219455419501372: 1950137.

Casapulla, C., L. Giresini and P. B. Lourenço (2017). "Rocking and Kinematic Approaches for Rigid Block Analysis of Masonry Walls: State of the Art and Recent Developments." Buildings **7**(3): 69.

Casapulla, C. and A. Maione (2017). "Free Damped Vibrations of Rocking Rigid Blocks as Uniformly Accelerated Motions." International Journal of Structural Stability and Dynamics **17**(06).

Casapulla, C., A. Maione and L. U. Argiento (2019b). "Performance-Based Seismic Analysis of Rocking Masonry Façades Using Non-Linear Kinematics with Frictional Resistances: A Case Study." International Journal of Architectural Heritage, 10.1080/15583058.2019.1674944.

Cattari, S., D. Camilletti, G. Magenes, C. F. Manzini, P. Morandi, E. Spacone, F. Cannizzaro, B. Calderoni, G. Camata, C. Marano, G. Occhipinti and A. E. S. Cordasco (2018). A Comparative Study On a 2-Storey Benchmark Case Study Through Nonlinear Seismic Analysis. 16th European Conference on Earthquake Engineering. Thessaloniki, Greece,

Degli Abbati, S., S. Cattari and S. Lagomarsino (2018). "Theoretically-based and practice-oriented formulations for the floor spectra evaluation." Earthquakes and Structures **15**(5): 565-581.

DeJong, M. J. (2009). Seismic Assessment Strategies for Masonry Structures. Doctor of Philosophy in Architecture: Building Technology. PhD Dissertation, MASSACHUSETTS INSTITUTE OF TECHNOLOGY.

Derakhshan, H., D. Y. Dizhur, M. C. Griffith and J. M. Ingham (2014). "Seismic Assessment of Out-of-plane Loaded Unreinforced Masonry Walls in Multi-Storey Buildings." Bulletin of the New Zealand Society for Earthquake Engineering **47**(2): 120-138.

Dimitri, R., L. De Lorenzis and G. Zavarise (2011). "Numerical study on the dynamic behavior of masonry columns and arches on buttresses with the discrete element method." Engineering Structures **33**(12): 3172-3188.

Dizhur, D., N. Ismail, C. Knox, R. Lumantarna and J. M. Ingham (2010). "Performance of Unreinforced and Retrofitted Masonry Buildings During the 2010 Darfield Earthquake." Bulletin of the New Zealand Society for Earthquake Engineering **43**(4): 321-339.

ElGawady, M. A., Q. Ma, J. W. Butterworth and J. Ingham (2011). "Effects of interface material on the performance of free rocking blocks." Earthquake Engineering & Structural Dynamics **40**(4): 375-392.

Eurocode 8 (2004). Design of structures for earthquake resistance. Part 1: General rules, seismic actions and rules for buildings. Brussels, Belgium: CEN., European Committee for Standardization,

Galvez, F., S. Segatta, M. Giaretton, K. Q. Walsh, I. Giongo and D. Dizhur (2018). FE and DE Modelling of Out-Of-Plane Two-Way Bending Behaviour of Unreinforced Masonry Walls. 16th European Conference on Earthquake Engineering. Thessaloniki, Greece,

Giaretton, M., D. Dizhur and J. M. Ingham (2016). "Dynamic testing of as-built clay brick unreinforced masonry parapets." Engineering Structures **127**: 676-685.

Giresini, L. (2017). Design Strategy for the Rocking Stability of Horizontally Restrained Masonry Walls. Proceedings of the 6th International Conference on Computational Methods in Structural Dynamics and Earthquake Engineering (COMPDYN 2015), 10.7712/120117.5620.18188**:** 2963-2979

Giresini, L., C. Casapulla, R. Denysiuk, J. Matos and M. Sassu (2018). "Fragility curves for free and restrained rocking masonry façades in one-sided motion." Engineering Structures **164**: 195-213.

Giresini, L., M. Fragiacomo and P. B. Lourenço (2015). "Comparison between rocking analysis and kinematic analysis for the dynamic out-of-plane behavior of masonry walls." Earthquake Engineering & Structural Dynamics **44**(13): 2359-2376.

Giresini, L. and M. Sassu (2016). "Horizontally restrained rocking blocks: evaluation of the role of boundary conditions with static and dynamic approaches." Bulletin of Earthquake Engineering **15**(1): 385-410.

Giresini, L., F. Solarino, O. Paganelli, D. V. Oliveira and M. Froli (2019). "ONE-SIDED rocking analysis of corner mechanisms in masonry structures: Influence of geometry, energy dissipation, boundary conditions." Soil Dynamics and Earthquake Engineering **123**: 357-370.

Gubana, A. and M. Melotto (2019). "Discrete-element analysis of floor influence on seismic response of masonry structures." Proceedings of the Institution of Civil Engineers - Structures and Buildings, 10.1680/jstbu.19.00099: 1-30.

Hess, R. L. (2007). Impacts of a M7.8 Southern San Andreas Earthquake on Unreinforced Masonry (URM) Buildings. The ShakeOut Scenario, Suplemental Study - Unreinforced Masonry (URM) Buildings, United States Geological Survey & California Geological Survey,

Housner, G. W. (1963). "The Behavior of Inverted Pendulum Structures During Earthquakes." Bulletin of the Seismological Society of America **53**(2): 403-417s.

Ishiyama, Y. (1982). "Motions of Rigid Bodies and Criteria For Overturning by Earthquake Excitations." Earthquake Engineering and Structural Dynamics **10**: 635-650.

Itasca (2013). 3DEC (3-Dimensional distinct element code). Minneapolis (MN)

Jing, L. and O. Stephansson (2007). Explicit Discrete Element Method for Block Systems – the Distinct Element Method. Fundamentals of Discrete Element Methods for Rock Engineering. **85:** 235-316.

Kalliontzis, D., S. Sritharan and A. Schultz (2016). "Improved Coefficient of Restitution Estimation for Free Rocking Members." Journal of Structural Engineering **142**(12): 06016002.

Lagomarsino, S. (1998). A new methodology for the post-earthquake investigation of ancient churches. 11th European Conference on Earthquake Engineering. Balkema, Rotterdam,

Lagomarsino, S. (2015). "Seismic assessment of rocking masonry structures." Bulletin of Earthquake Engineering **13**(1): 97-128.

Lemos, J. V. and A. Campos Costa (2017). "Simulation of Shake Table Tests on Out-Of-Plane Masonry Buildings. Part (V): Discrete Element Approach." International Journal of Architectural Heritage **11**(1): 117-124.

Lipo, B. and G. de Felice (2016). Smooth-Rocking Oscillator under Natural Accelerograms. ECCOMAS Congress 2016 - VII European Congress on Computational Methods in Applied Sciences and Engineering. V. P. M. Papadrakakis, G. Stefanou, V. Plevris (eds. Crete Island, Greece,

Lipscombe, P. R. and S. Pellegrino (1993). "Free Rocking of Prismatic Blocks." Journal of Engineering Mechanics **119**(7): 1387-1410.

Lorig, L. J. and R. D. Hart (1993). Block dynamics modeling in support of seismic design. Dynamic Analysis and Design Considerations for High-Level Nuclear Waste Repositories. H. Q. (ed.). New York, ASCE:**:** 228-242

MathWorks (2008). "MATLAB User´s Manual. ."

McNeel, R. and Associates (2014). Rhinoceros 5,

Menon, A. and G. Magenes (2011). "Definition of Seismic Input for Out-of-Plane Response of Masonry Walls: I. Parametric Study." Journal of Earthquake Engineering **15**(2): 165-194.

Meriggi, P., G. de Felice, S. De Santis, F. Gobbin, A. Mordanova and B. Pantò (2019). "Distinct Element Modelling of Masonry Walls under Out-Of-Plane Seismic Loading." International Journal of Architectural Heritage **13**(7): 1110-1123.

Mordanova, A., G. de Felice and A. Genoese (2017). Assessment of the stability condition of the claudio aqueduct. 3rd International Conference on Protection of Historical Constructions. Lisbon, Portugal,

NZS1170.5 (2004). Structural design actions, Part 5: earthquake actions—New Zealand. NZS 1170.5:2004. Standards New Zealand (NZS), Standards New Zealand (NZS) Technical Committee BD-006-04-11, Wellington, New Zealand.,

Olcese, S. (2018). Use of discrete element modelling for the seismic assessment of a benchmark case study masonry structure. Corso di Laurea in Ingegneria Edile – Architettura. Master Thesis, Università degli Studi di Genova.

Papantonopoulos, C., I. N. Psycharis, D. Y. Papastamatiou, J. V. Lemos and H. P. Mouzakis (2002). "Numerical prediction of the earthquake response of classical columns using the distinct element method." Earthquake Engineering & Structural Dynamics **31**(9): 1699-1717.

Priestley, M. J. N. (1985). "Seismic Behaviour of Unreinforced Masonry Walls." Bulletin of The New Zealand National Society for Earthquake Engineering **18**(2).

Psycharis, I. N. and P. C. Jennings (1983). "Rocking of Slender Rigid Bodies Allowed to Uplift." Earthquake Engineering and Structural Dynamics **11**: 57-76.

Psycharis, I. N., J. V. Lemos, D. Y. Papastamatiou, C. Zambas and C. Papantonopoulos (2003). "Numerical study of the seismic behaviour of a part of the Parthenon Pronaos." Earthquake Engineering & Structural Dynamics **32**(13): 2063-2084.

Pulatsu, B., F. Gencer and E. Erdogmus (2020). "Study of the effect of construction techniques on the seismic capacity of ancient dry-joint masonry towers through DEM." European Journal of Environmental and Civil Engineering, 10.1080/19648189.2020.1824823: 1-18.

Shawa, O. A., G. de Felice, A. Mauro and L. Sorrentino (2012). "Out-of-Plane Seismic Behaviour of Rocking Masonry Walls." Journal of Earthquake Engineering and Structural Dynamics **5**(2): 253-271.

Sigurdsson, G. Ö., R. Rupakhety and S. Ólafsson (2019). "A Study of Rigid Blocks Rocking Against Rigid Walls." **47**: 323-334.

Sorrentino, L., O. AlShawa and L. D. Decanini (2011). "The relevance of energy damping in unreinforced masonry rocking mechanisms. Experimental and analytic investigations." Bulletin of Earthquake Engineering **9**(5): 1617-1642.

Sorrentino, L., S. Kunnath, G. Monti and G. Scalora (2008). "Seismically induced one-sided rocking response of unreinforced masonry façades." Engineering Structures **30**(8): 2140-2153.

Ther, T. and L. P. Kollár (2016). "Refinement of Housner's model on rocking blocks." Bulletin of Earthquake Engineering **15**(5): 2305-2319.

Tomassetti, U., F. Graziotti, L. Sorrentino and A. Penna (2019). "Modelling rocking response via equivalent viscous damping." Earthquake Engineering & Structural Dynamics, 10.1002/eqe.3182.

Table 1: Selected ground motions

Event – Station (Component)	Date	M_w	D [km]	Soil Type	PGA [g]	PGV [cm/s]	PGD [cm]	Δt [s]
Bucarest, Romania - Building Research Institute (BUCAR0)	March/4/1977	7.5	150	D	0.21	73.6	24.4	16.2
Northridge, CA, USA – Rinaldi Receiving Station (RRS228)	January/17/1994	6.7	0.1	C	0.84	166.1	28.8	14.9
Nahanni, Canada – Site 1 (1ST280)	December/23/1985	6.8	0.1	A	1.1	46.1	14.6	20.5
Christchurch, NZ - Heathcote Valley School (HVSC1)	February/22/2011	6.3	4	C	1.58	106.6	21.77	29.0

M_w = Moment magnitude

D = Distance from the surface projection of the source

Soil type = According to Eurocode 8 (2004)

Peak ground: PGA = Acceleration, PGV = Velocity, PGD = Displacement

Δt = Duration

Table 2: Weighted Mean Error as in equation 10.

	SDOF		2DOF		3DOF		4DOF		5DOF	
	BUCAR0	RRS228	BUCAR0	RRS228	BUCAR0	RRS228	BUCAR0	RRS228	BUCAR0	RRS228
Acceleration Top Response	0.344	0.407	0.309	0.343	0.305	0.331	0.298	0.326	0.292	0.323
Response Spectra	0.140	0.152	0.082	0.093	0.063	0.074	0.056	0.066	0.062	0.062
Power Spectra	0.273	0.231	0.160	0.141	0.133	0.117	0.119	0.108	0.129	0.105

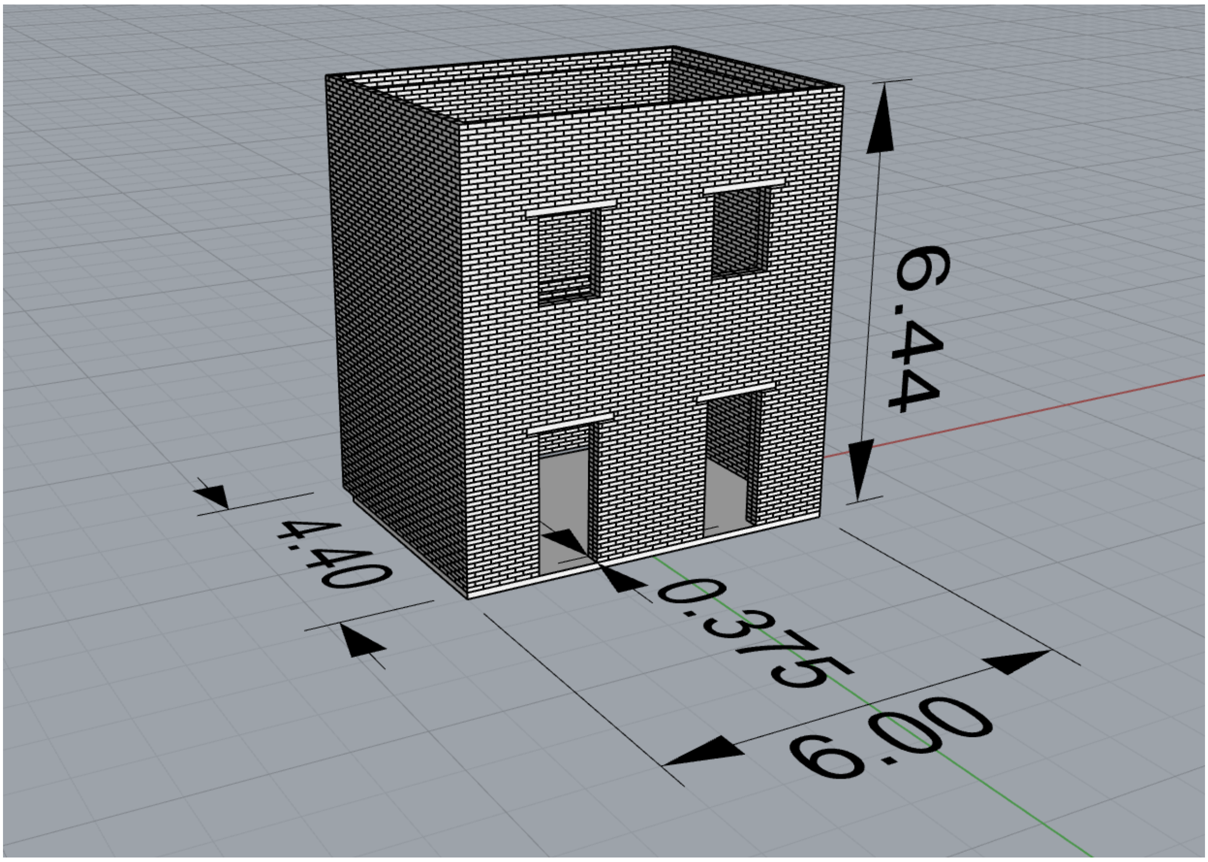

(a) Rhinoceros® (Dimensions in m)

Figure 1: Geometrical model of the two-storey case study building

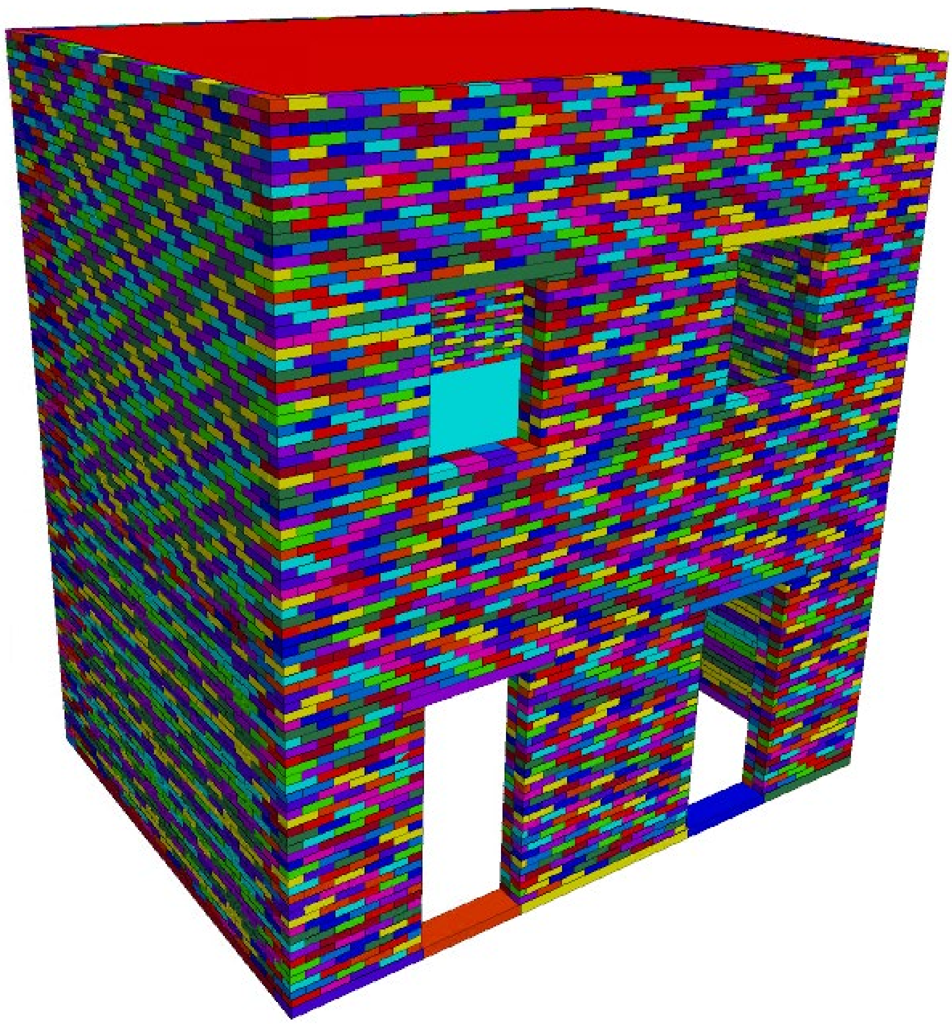

(b) DEM

Figure 1: Geometrical model of the two-storey case study building

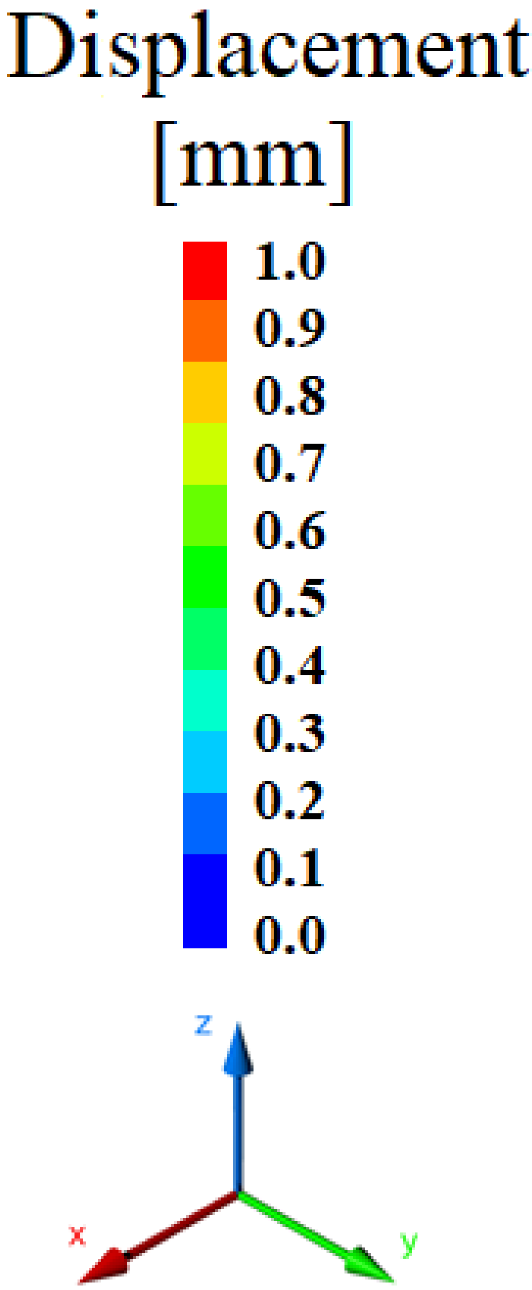

Figure 2: First and second modal shapes and periods in the *Y* direction of the complete and the simplified structure calculated using DEM modal analysis

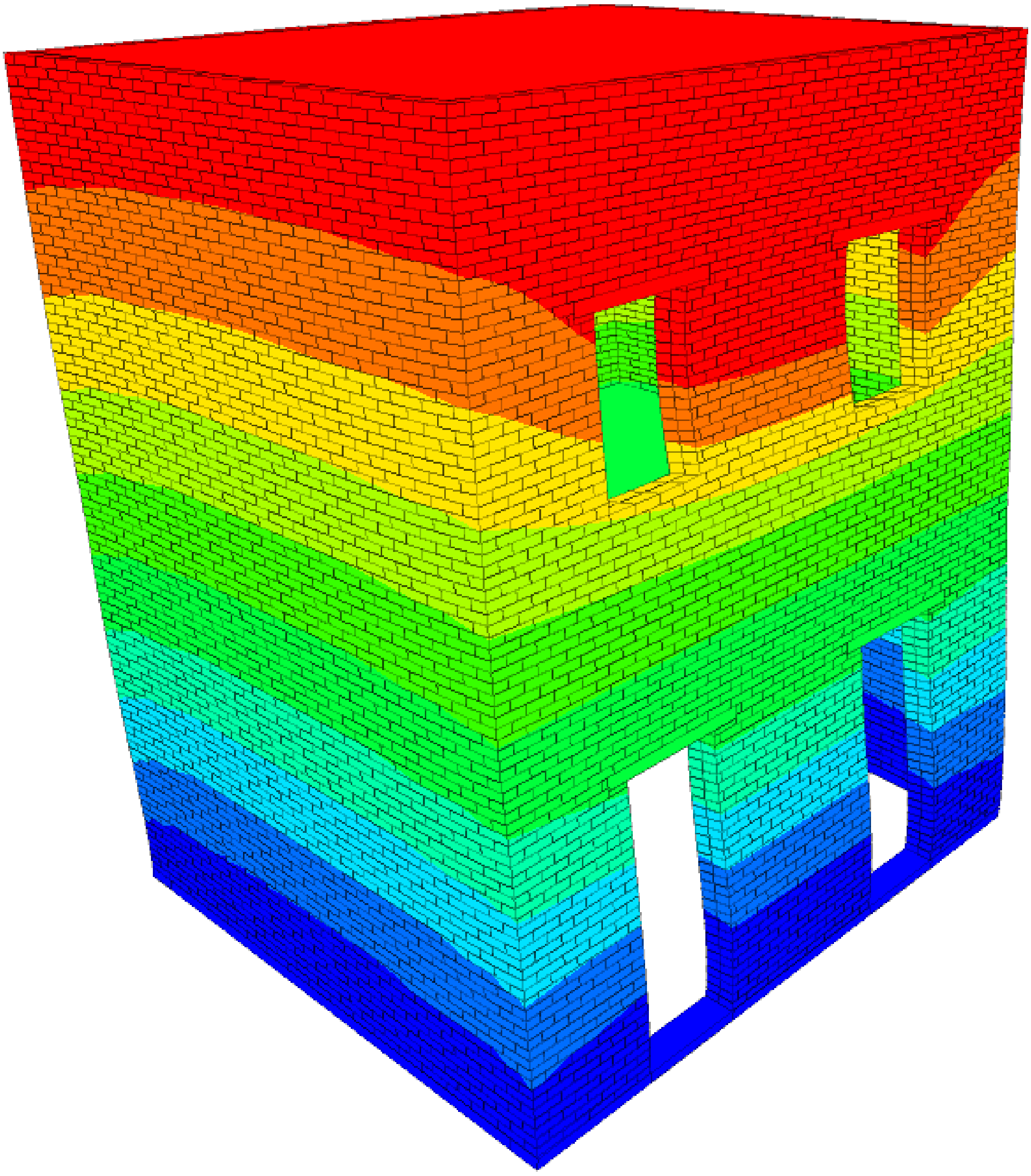

(a) 1st mode of CBDEM (T=0.25 s)

Figure 2: First and second modal shapes and periods in the *Y* direction of the complete and the simplified structure calculated using DEM modal analysis

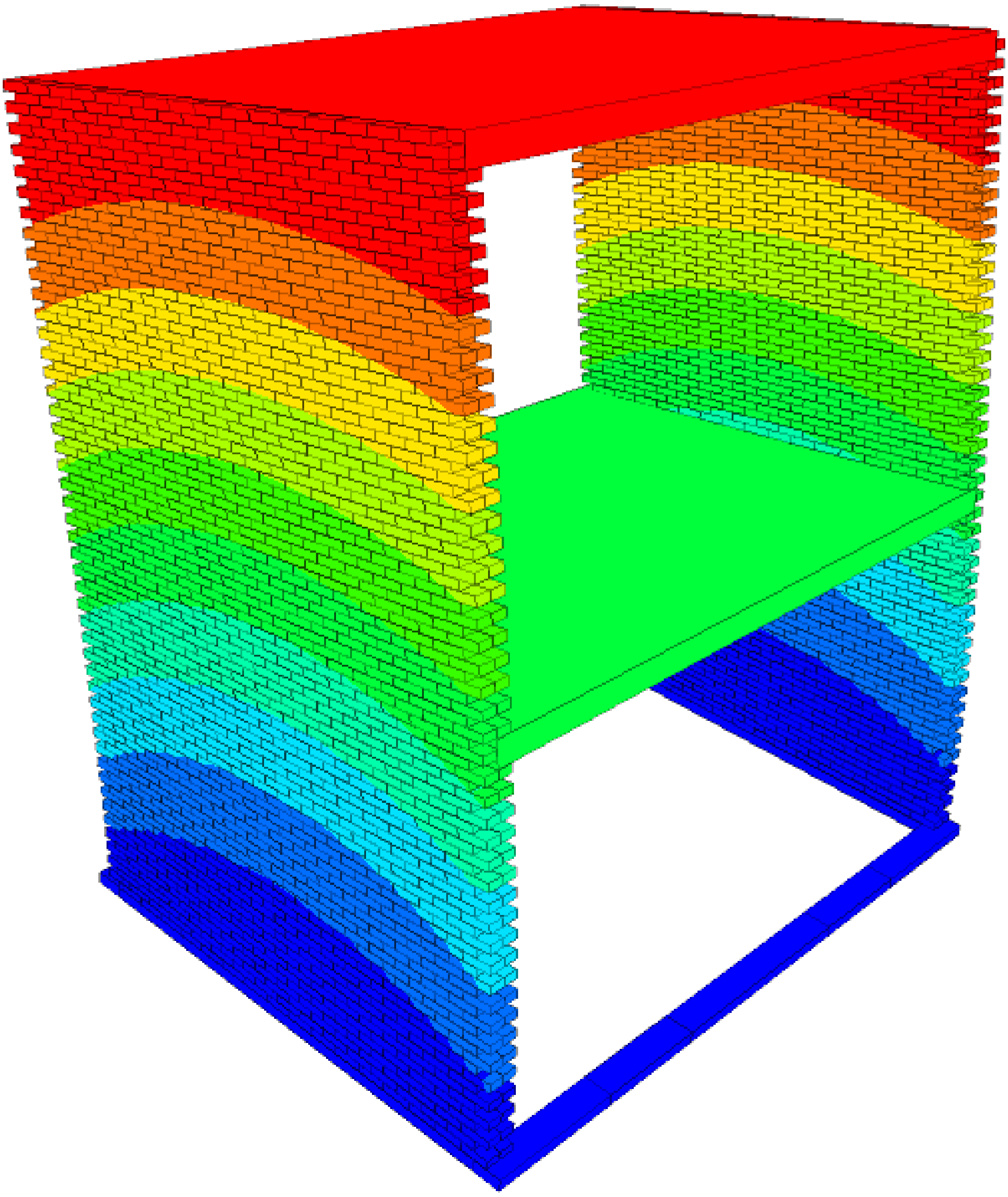

(b) 1st mode of SBDEM (T=0.27 s)

Figure 2: First and second modal shapes and periods in the *Y* direction of the complete and the simplified structure calculated using DEM modal analysis

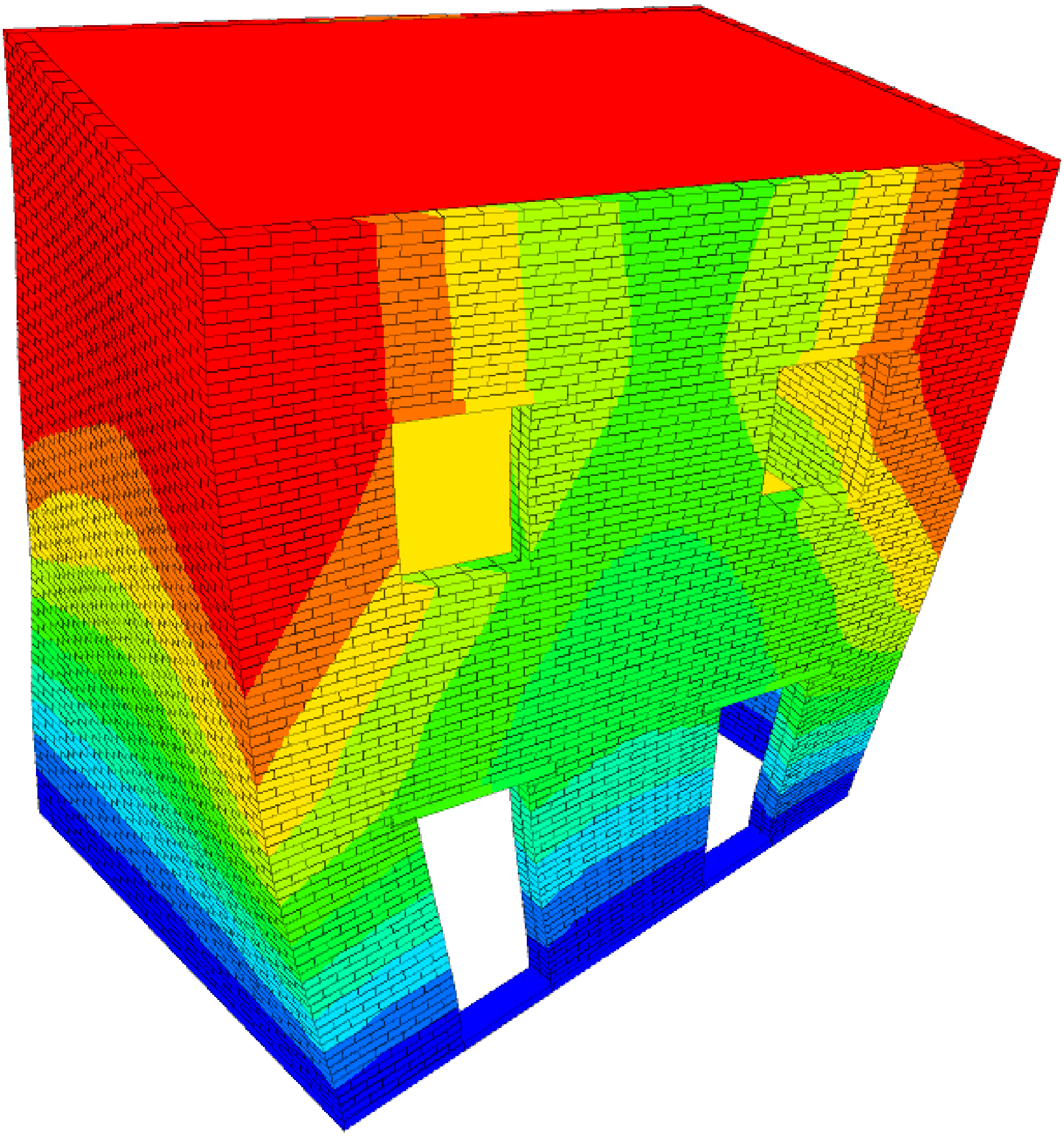

(c) 2nd mode of CBDEM (T=0.16 s)

Figure 2: First and second modal shapes and periods in the *Y* direction of the complete and the simplified structure calculated using DEM modal analysis

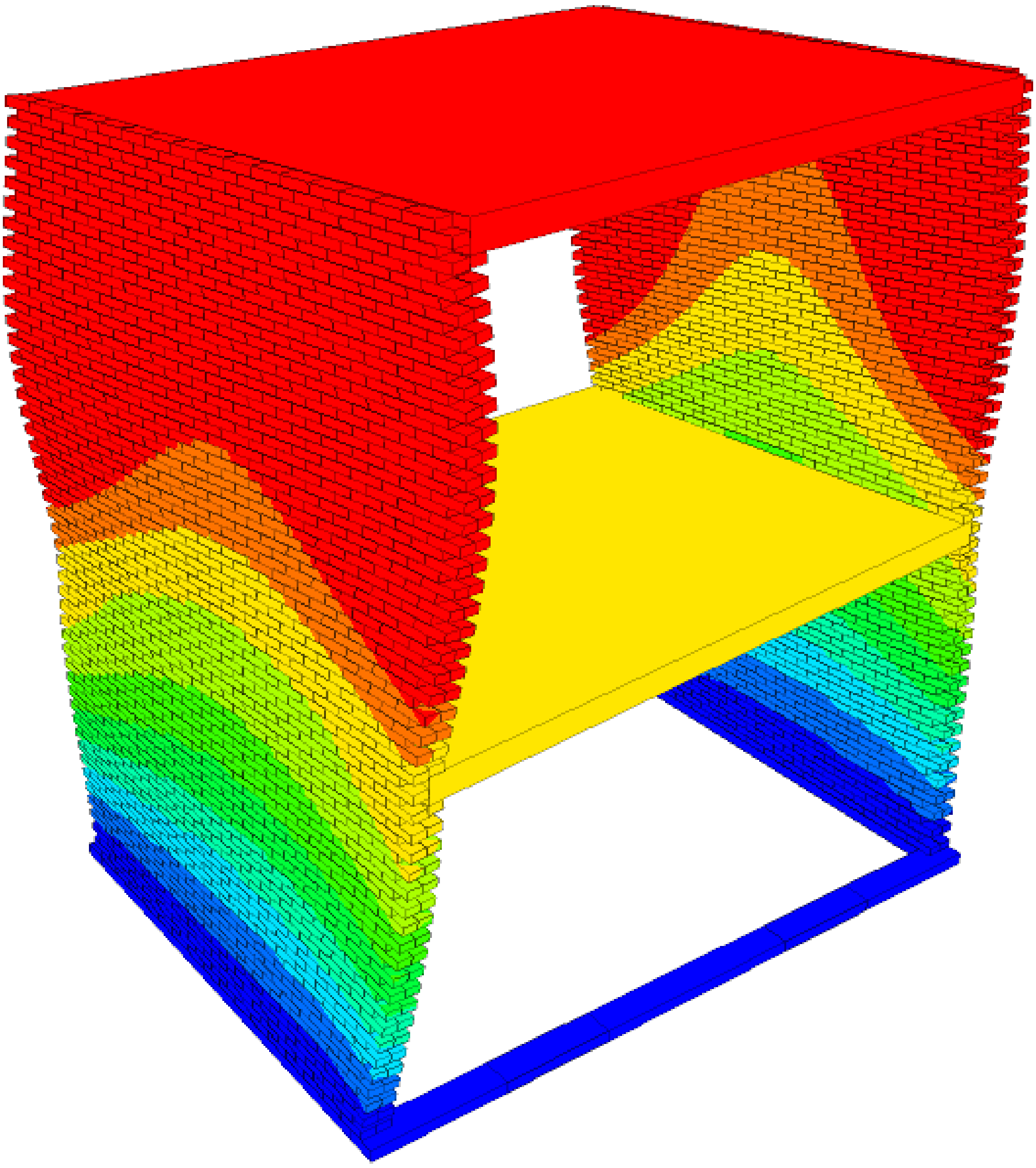

(d) 2nd mode of SBDEM (T=0.17 s)

Figure 2: First and second modal shapes and periods in the *Y* direction of the complete and the simplified structure calculated using DEM modal analysis

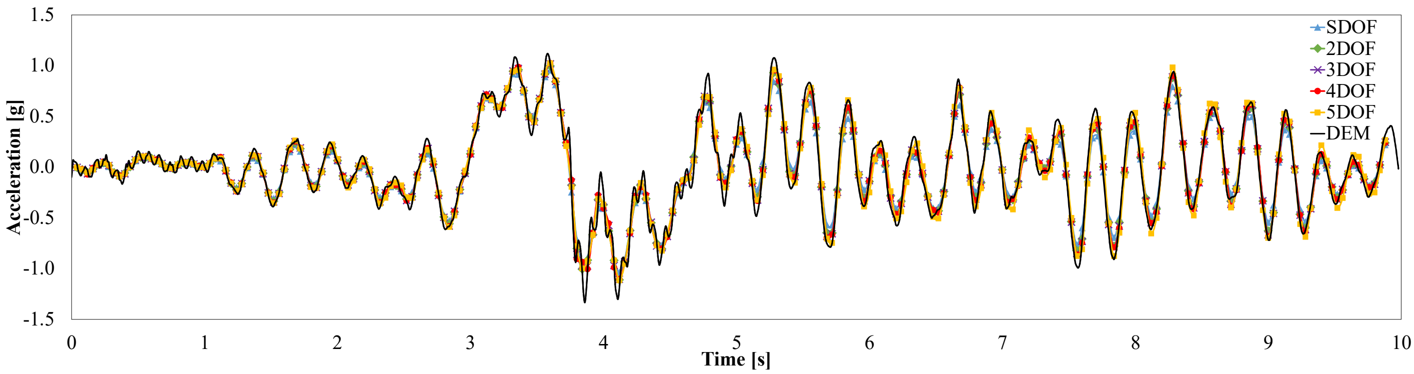

(a) Time-history response

Figure 3: Comparison between the seismic response of the SBDEM and SMDOF for BUCAR0 earthquake.

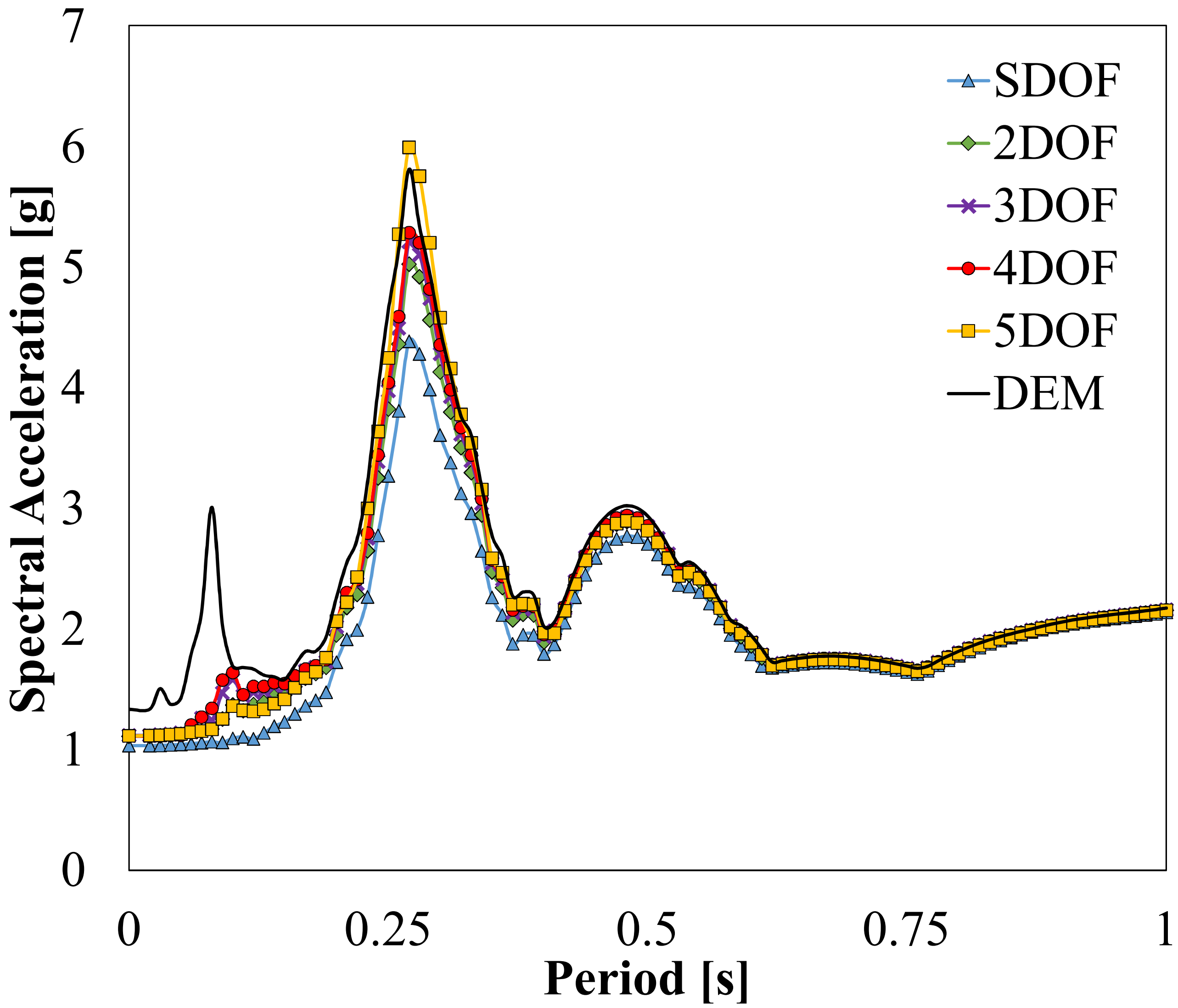

(b) Response Spectra

Figure 3: Comparison between the seismic response of the SBDEM and SMDOF for BUCAR0 earthquake.

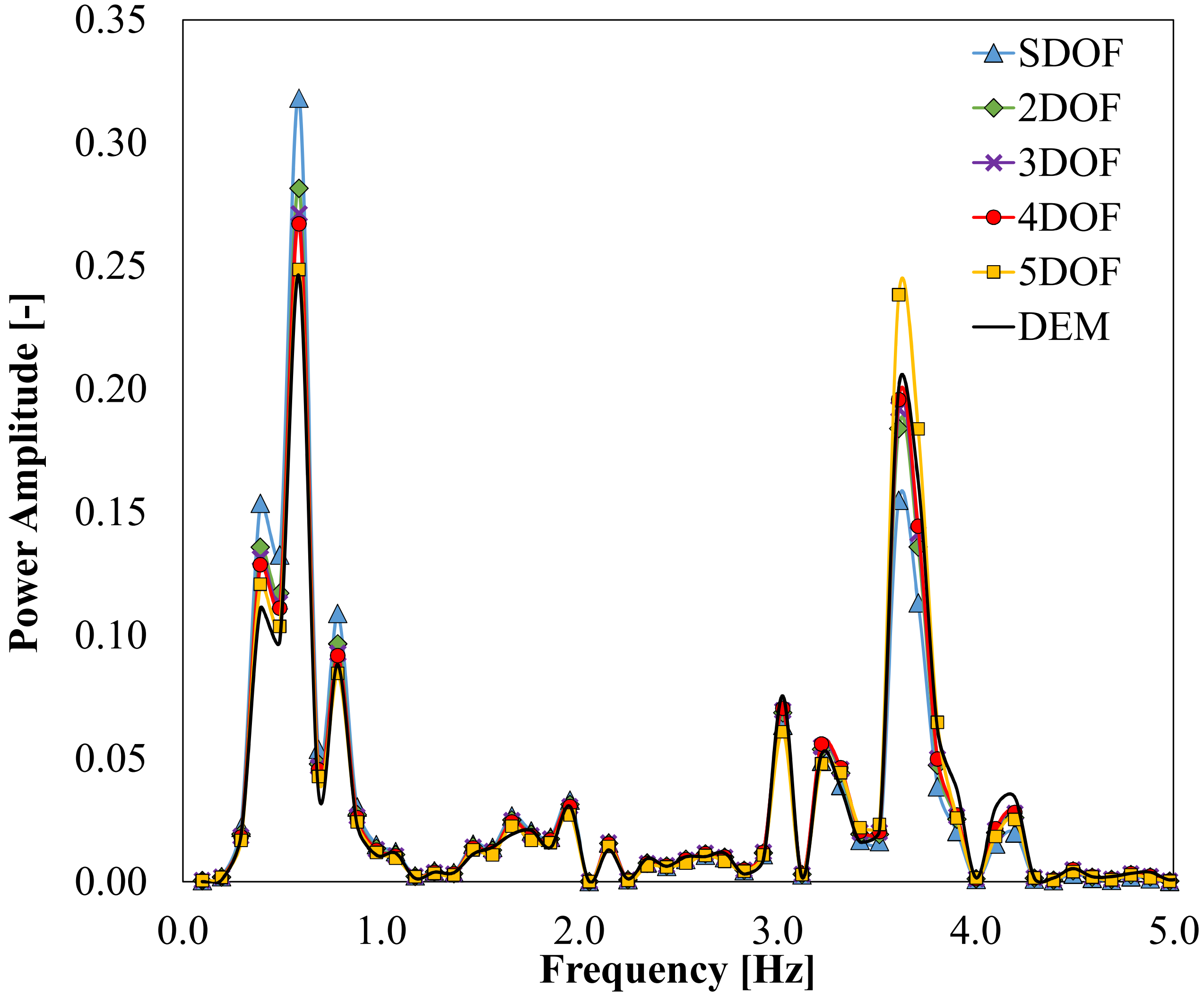

(c) Power Spectra

Figure 3: Comparison between the seismic response of the SBDEM and SMDOF for BUCAR0 earthquake.

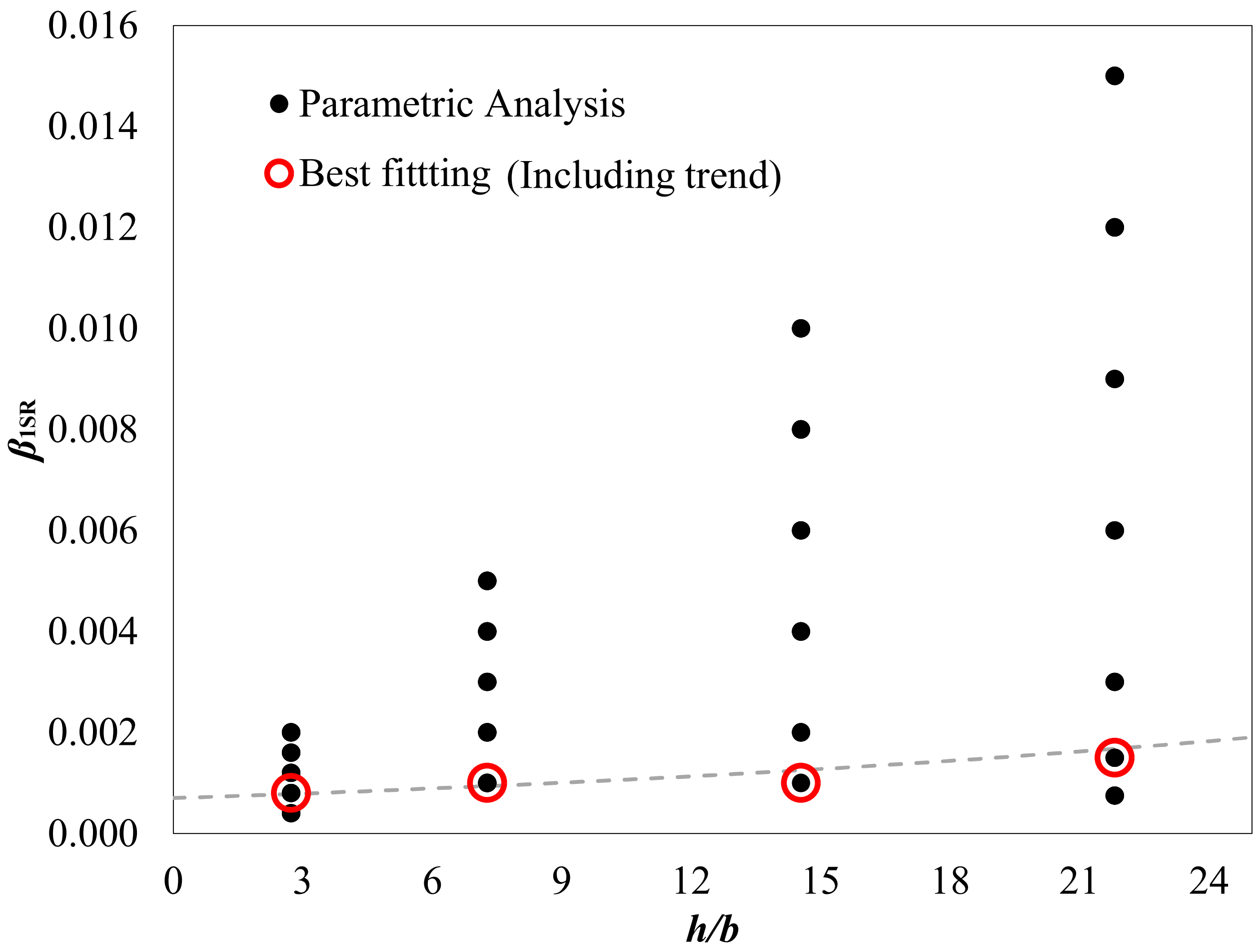

(a) Values of β_{1SR} for walls with b = 0.11 m, E = 1800 MPa and different values of h/b.

Figure 4: Parametric studies.

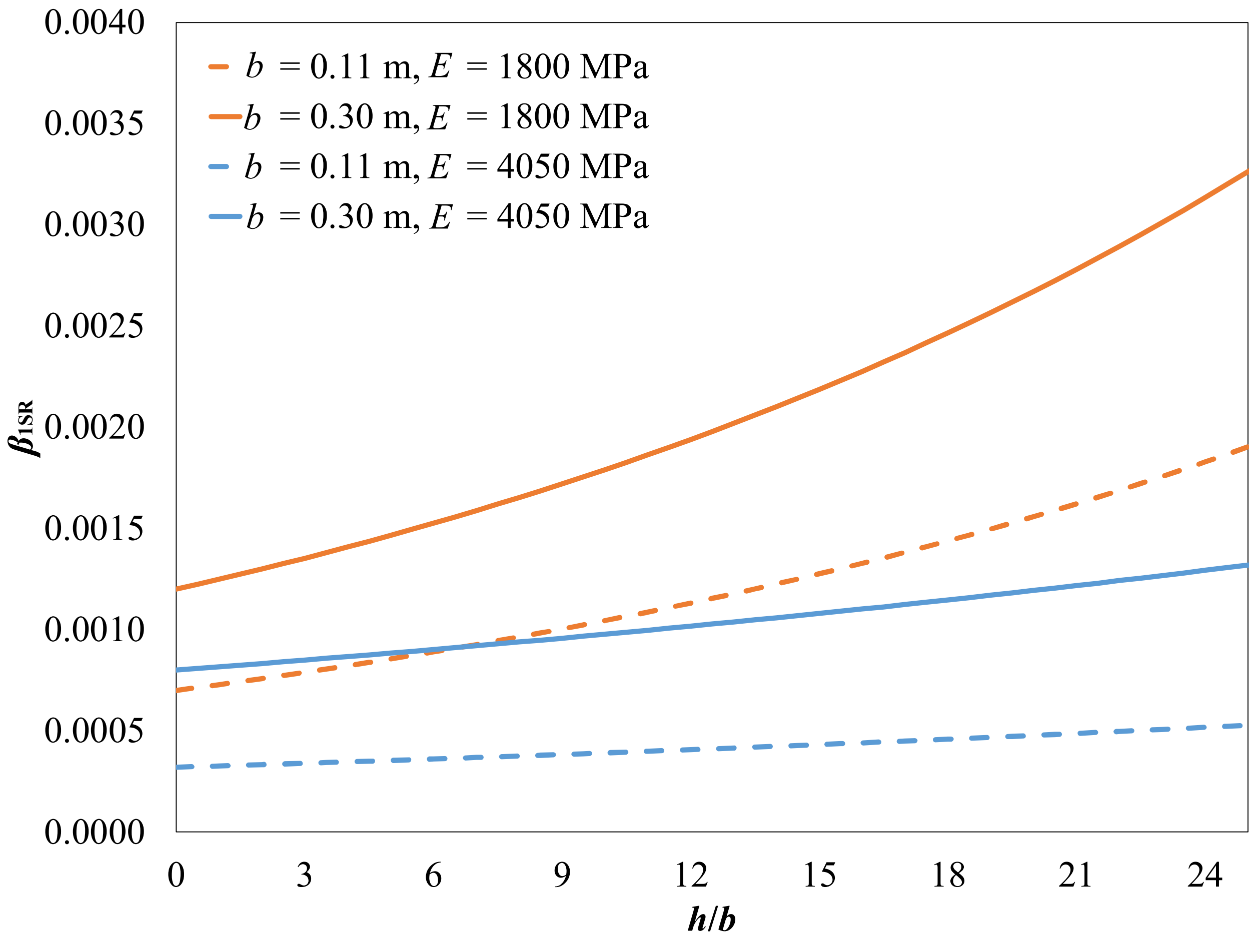

(b) Best fitting β_{1SR} for different values of E and geometry variations

Figure 4: Parametric studies.

(a) Experimental setup (Sorrentino et al., 2011)

Figure 5: Experimental testing from Sorrentino et al. (2011) and simulations using 3DEC

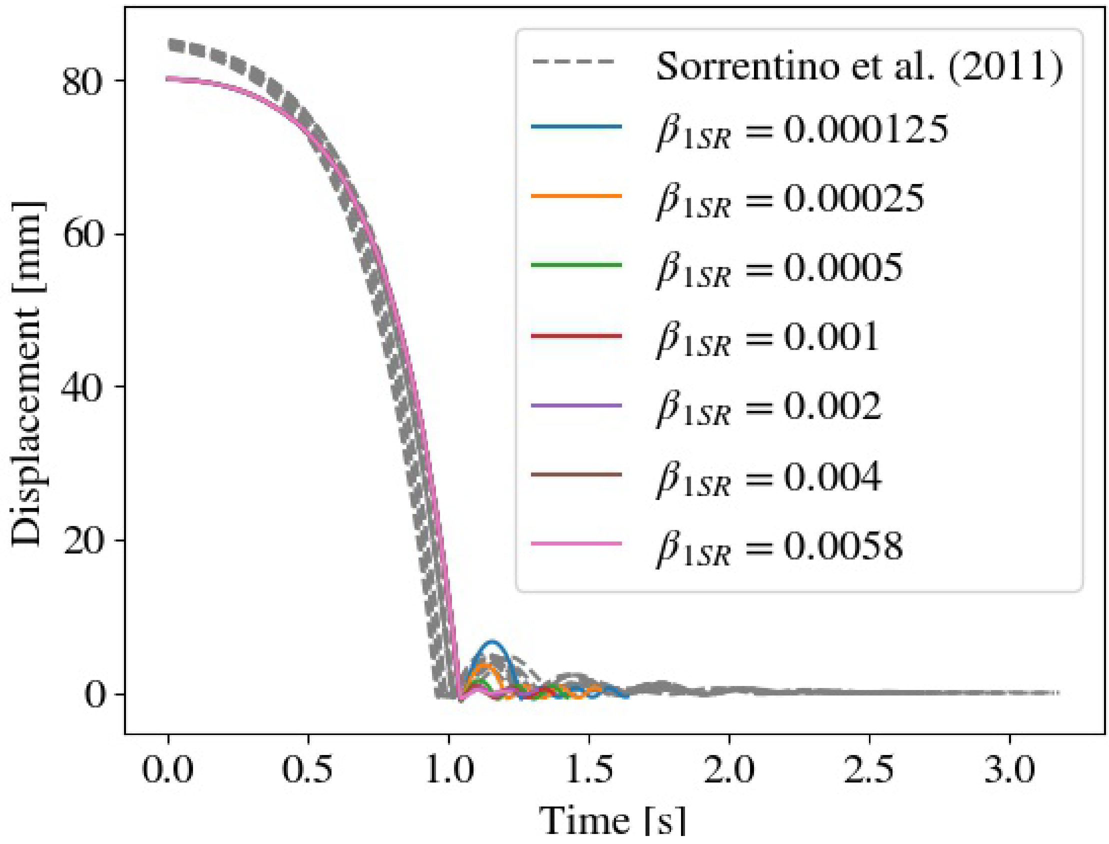

(b) Complete time-history

Figure 5: Experimental testing from Sorrentino et al. (2011) and simulations using 3DEC

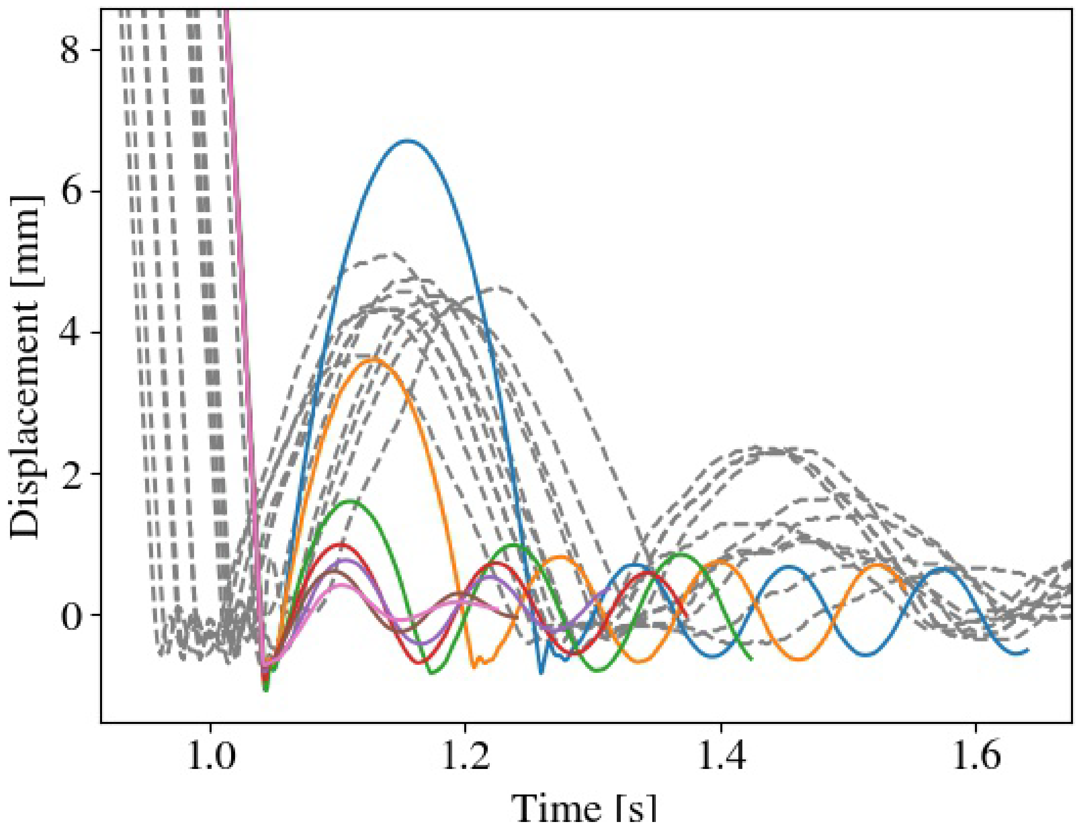

(c) Expanded view between 0.9 s and 1.9 s

Figure 5: Experimental testing from Sorrentino et al. (2011) and simulations using 3DEC

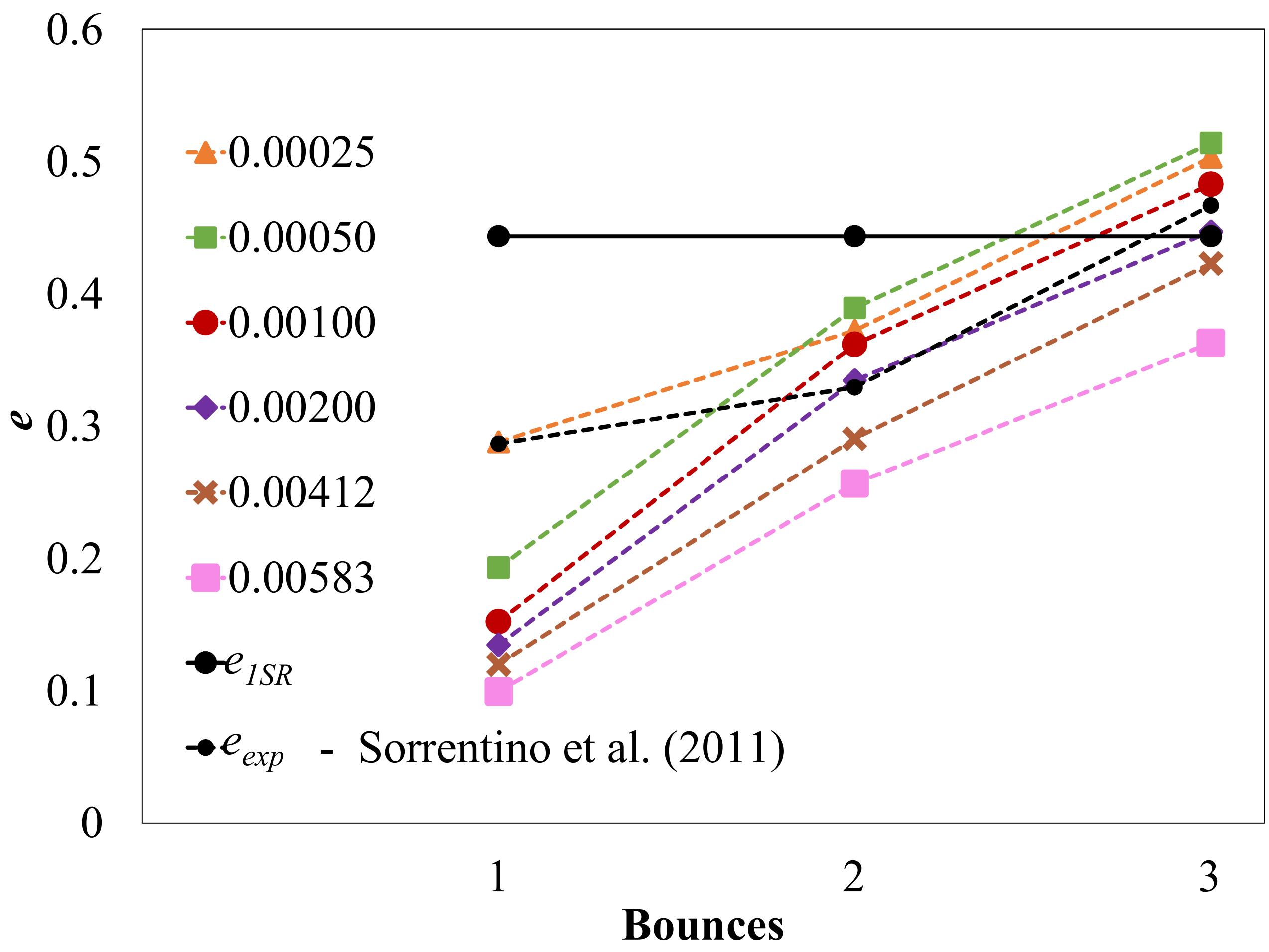

(d) Values of e_{exp} for different simulations using β_{1SR} compared to e_{1SR} and experimental testing

Figure 5: Experimental testing from Sorrentino et al. (2011) and simulations using 3DEC

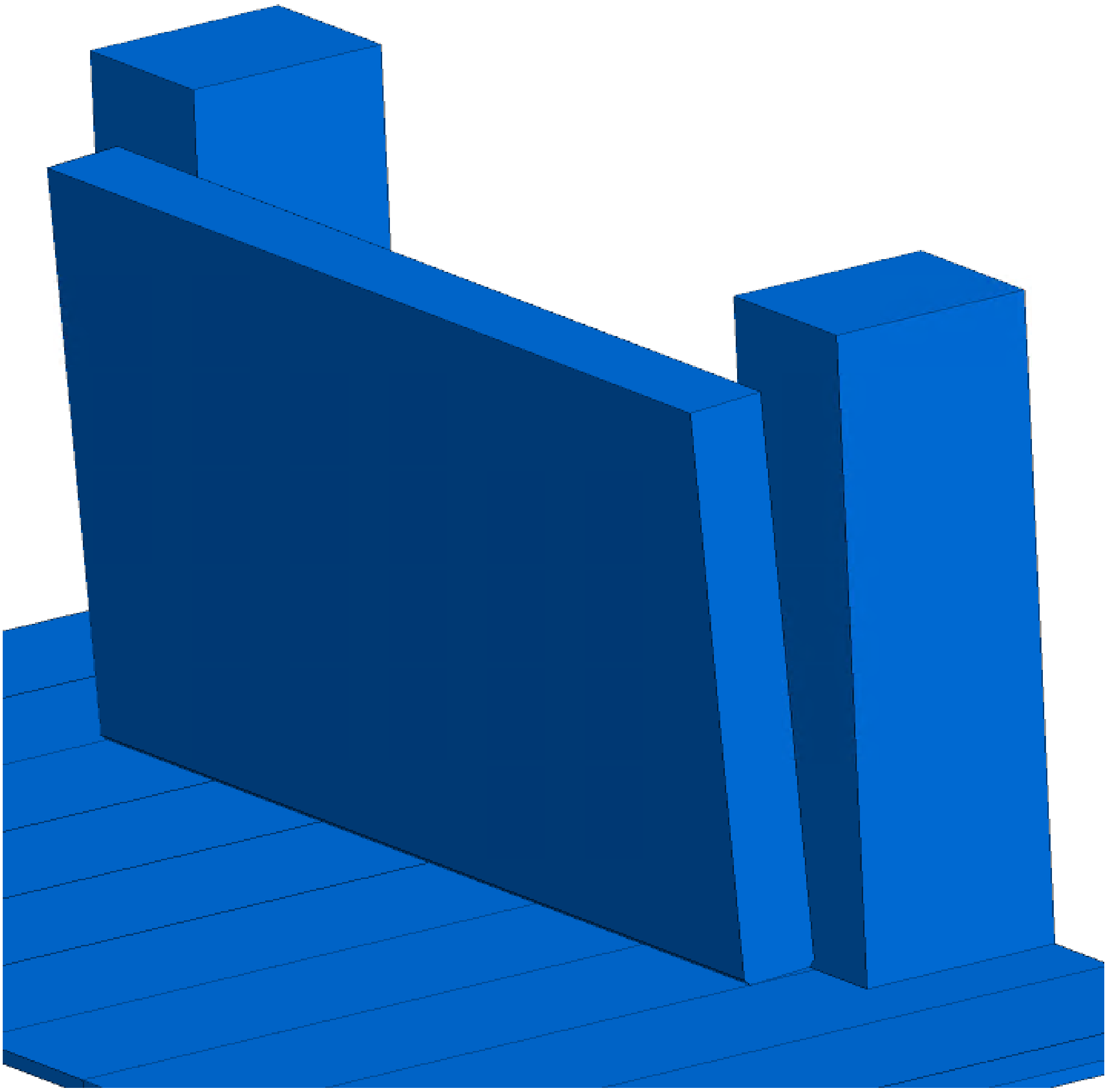

(a) DEM model

Figure 6: Comparison of top displacement between experiments and DEM simulation.

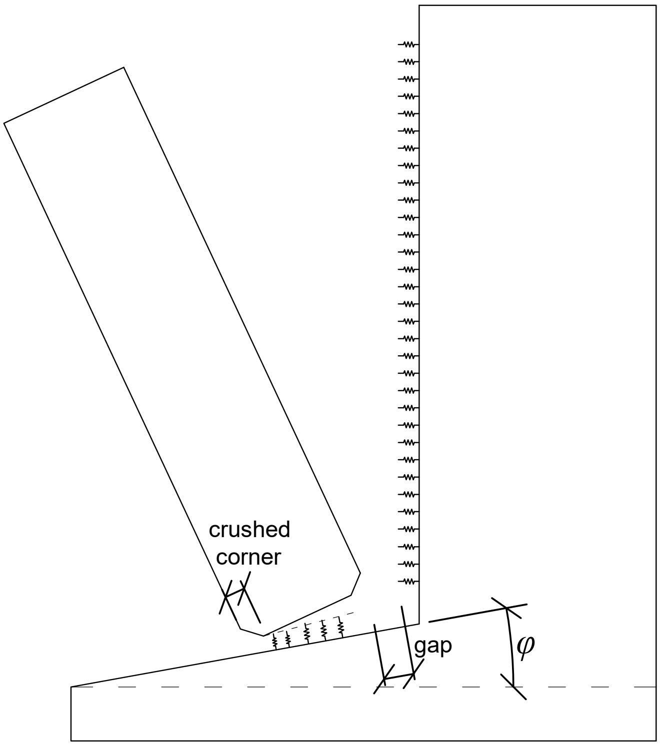

(b) Diagram of tilted rocking facade

Figure 6: Comparison of top displacement between experiments and DEM simulation.

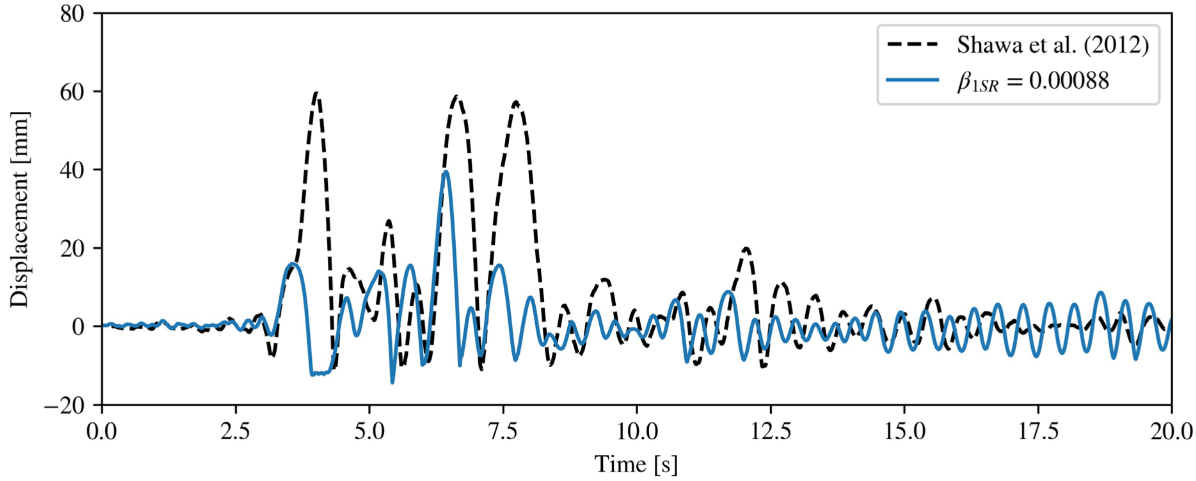

(c) BagnirWE, $\varphi = 0.191^\circ$

Figure 6: Comparison of top displacement between experiments and DEM simulation.

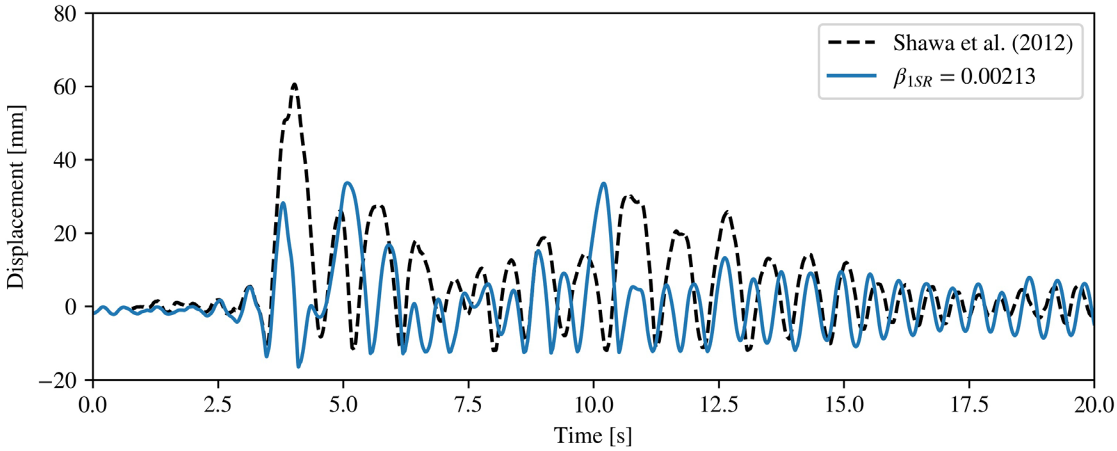

(d) SturWE, $\varphi = 0.210^\circ$

Figure 6: Comparison of top displacement between experiments and DEM simulation.

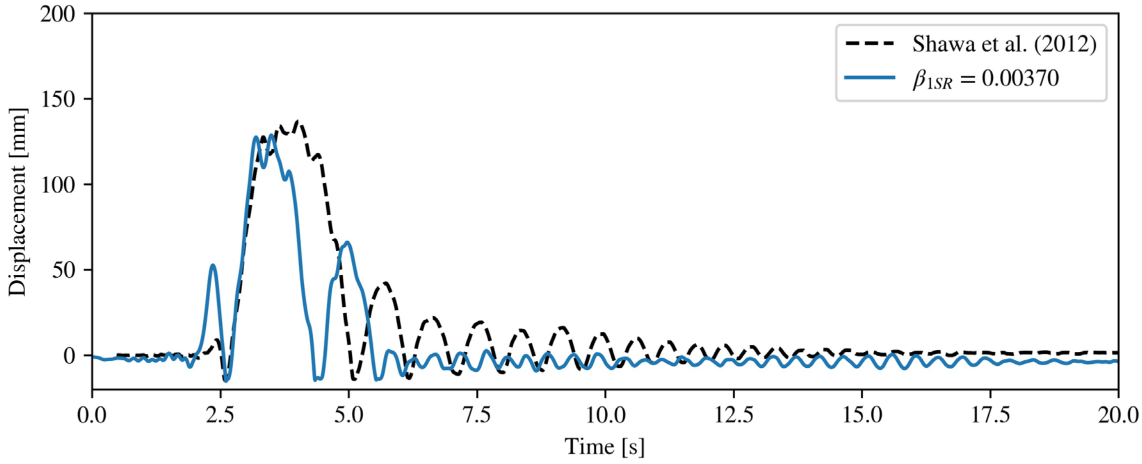

(e) R1168EW, $\varphi = 0.272^\circ$

Figure 6: Comparison of top displacement between experiments and DEM simulation.

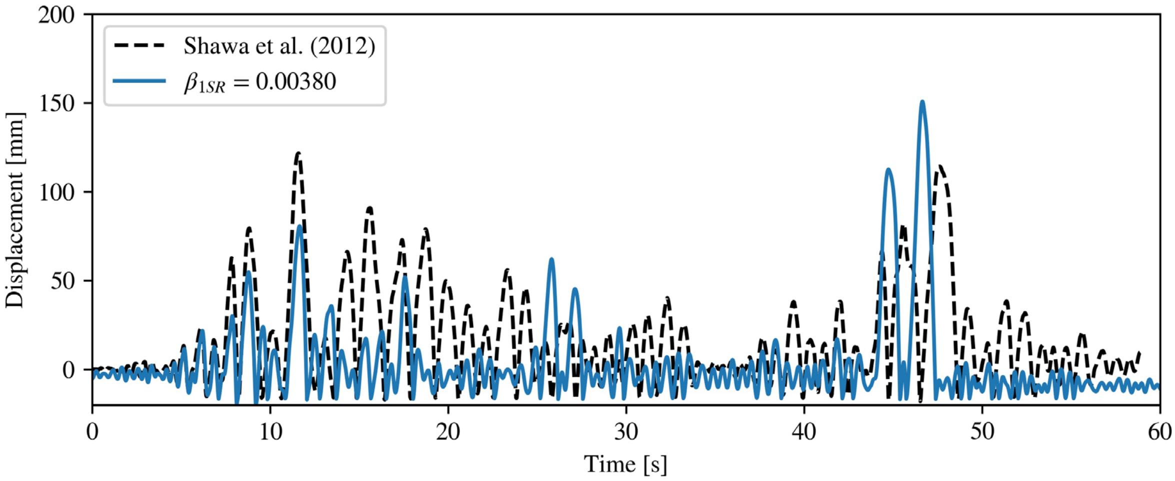

(f) CalitWE, $\varphi = 0.348^\circ$

Figure 6: Comparison of top displacement between experiments and DEM simulation.

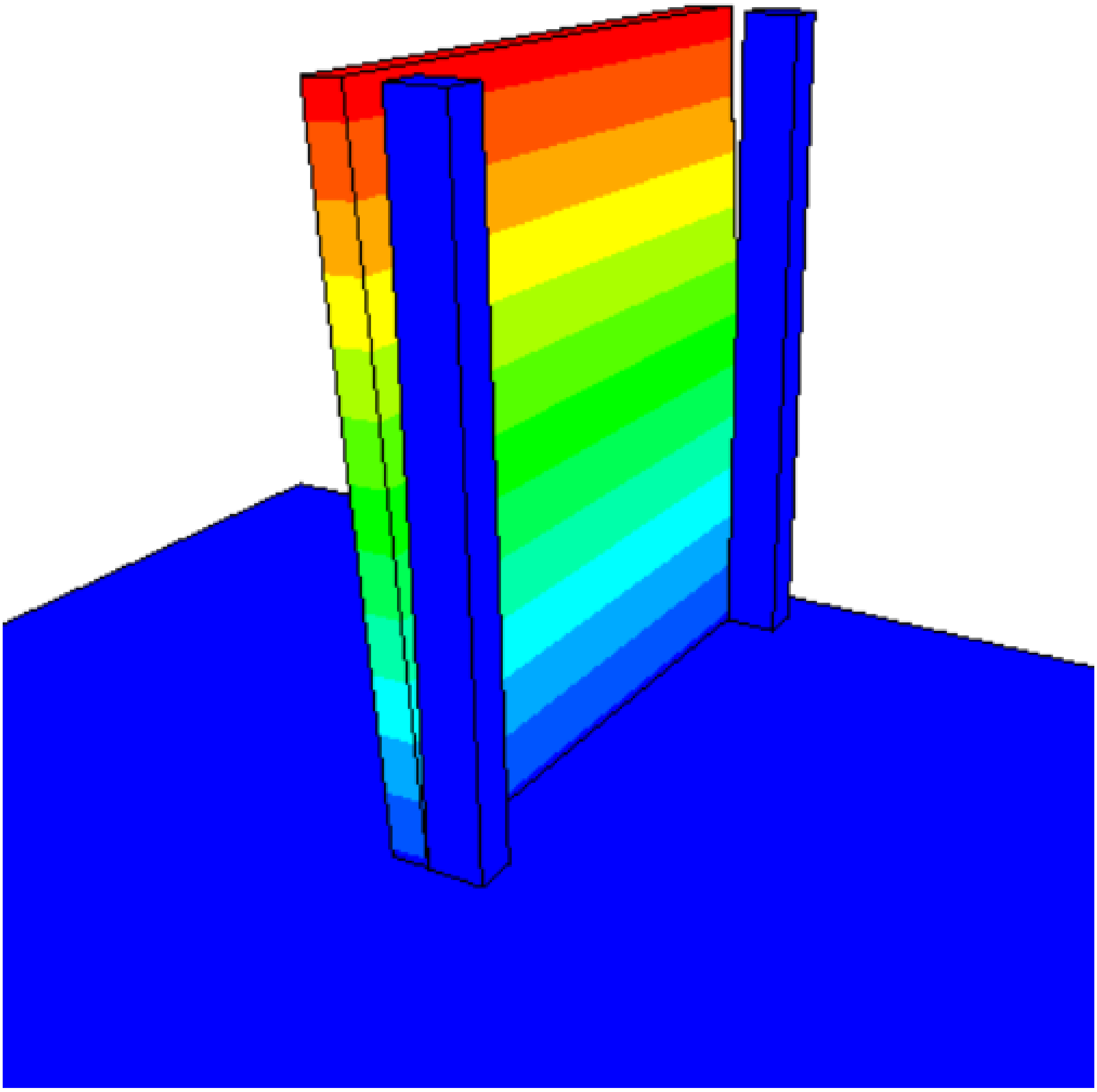

(a) W1

Figure 7: DEM modelling of rocking façade and return walls with associated block and spring interaction scheme (Colours represent displacement magnitude without scale).

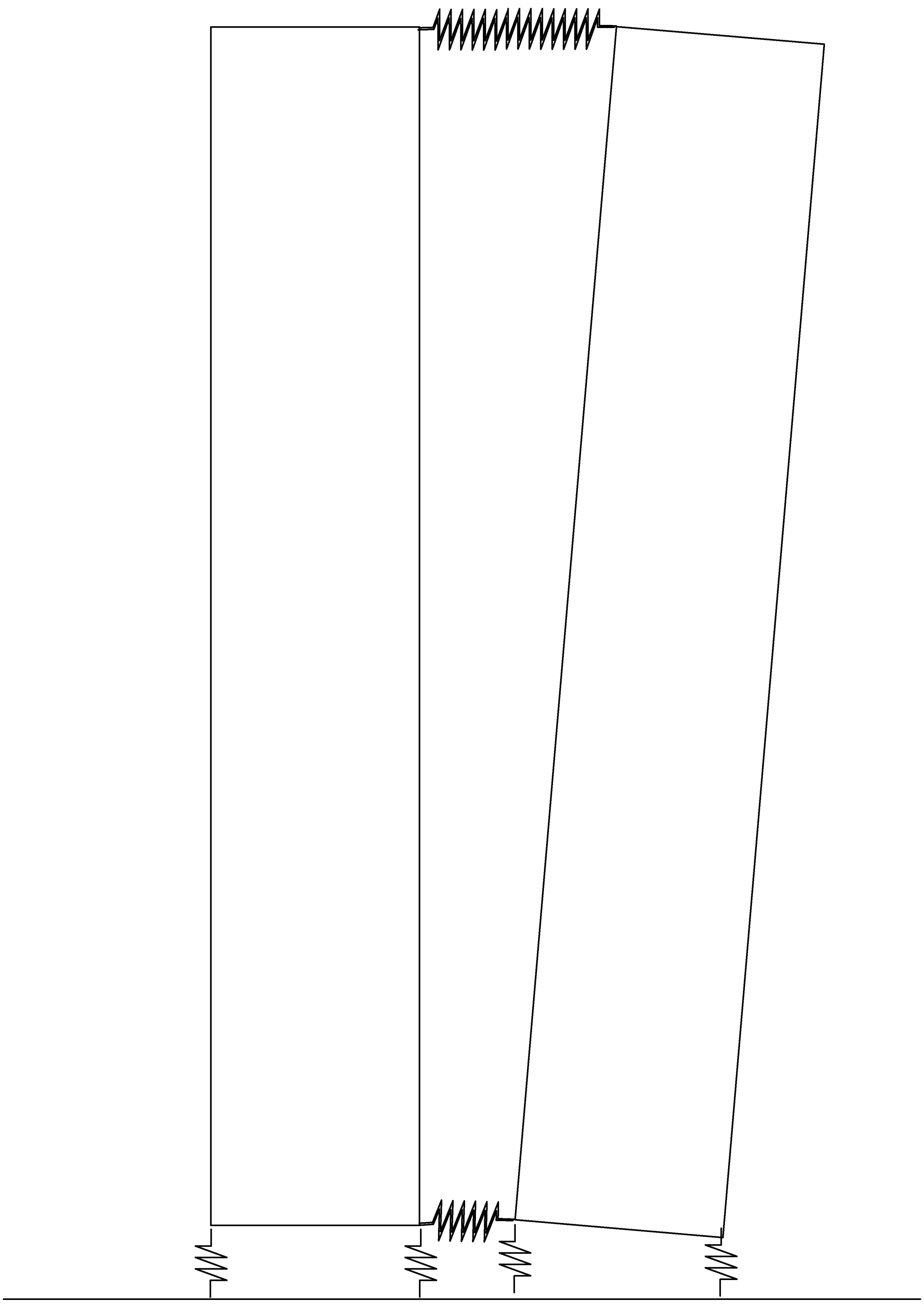

(a) W1

Figure 7: DEM modelling of rocking façade and return walls with associated block and spring interaction scheme (Colours represent displacement magnitude without scale).

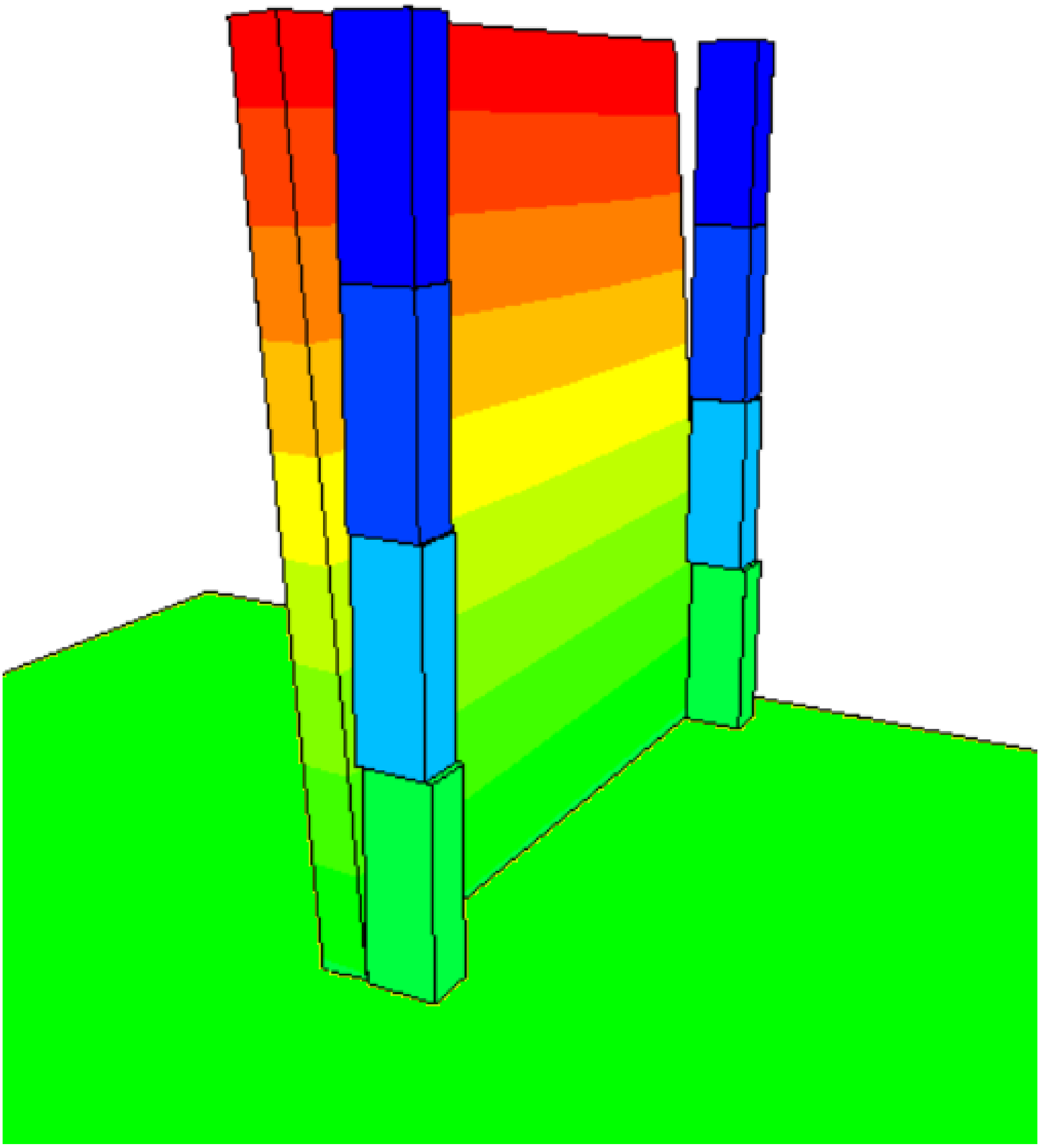

(b) W2

Figure 7: DEM modelling of rocking façade and return walls with associated block and spring interaction scheme (Colours represent displacement magnitude without scale).

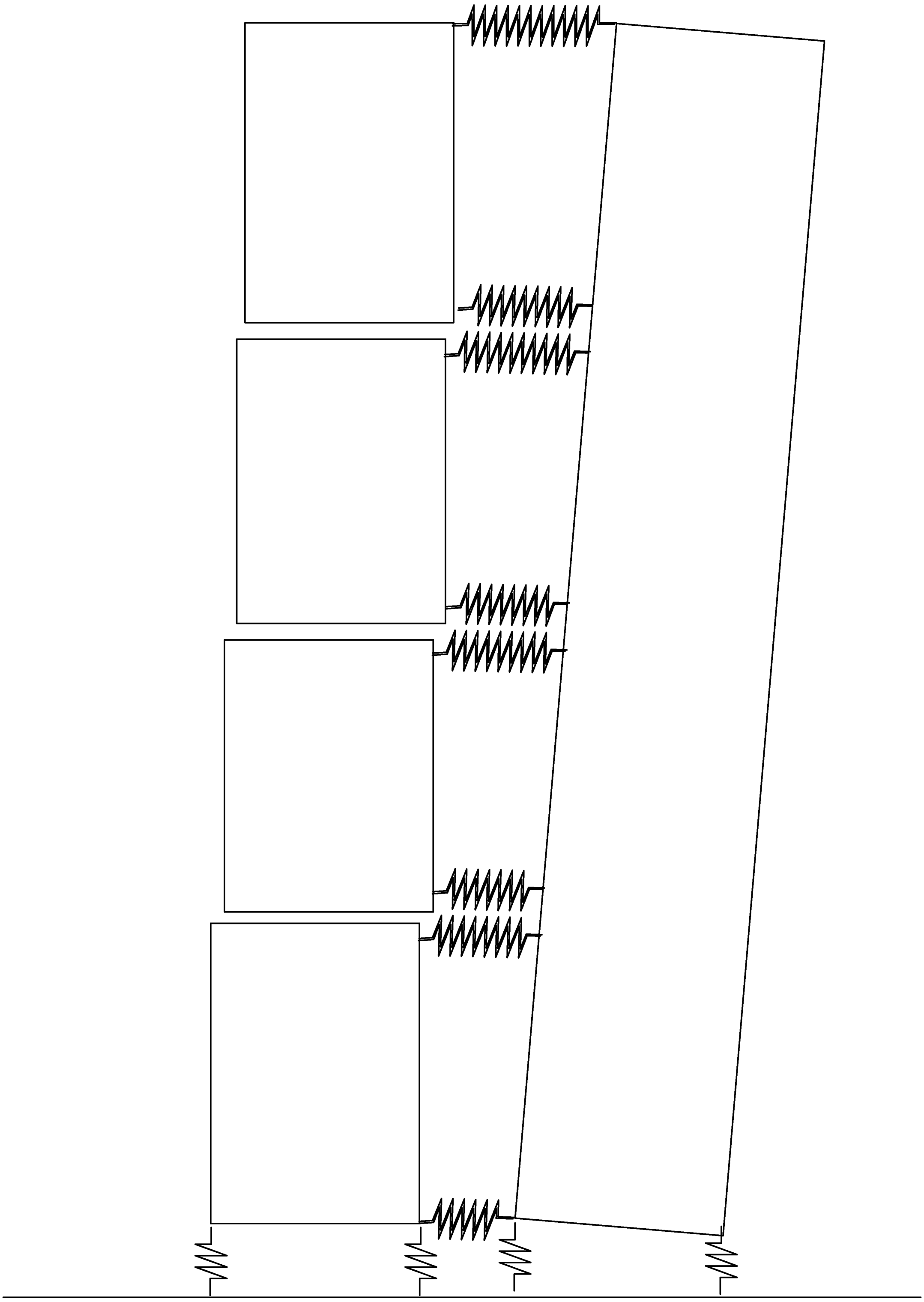

(b) W2

Figure 7: DEM modelling of rocking façade and return walls with associated block and spring interaction scheme (Colours represent displacement magnitude without scale).

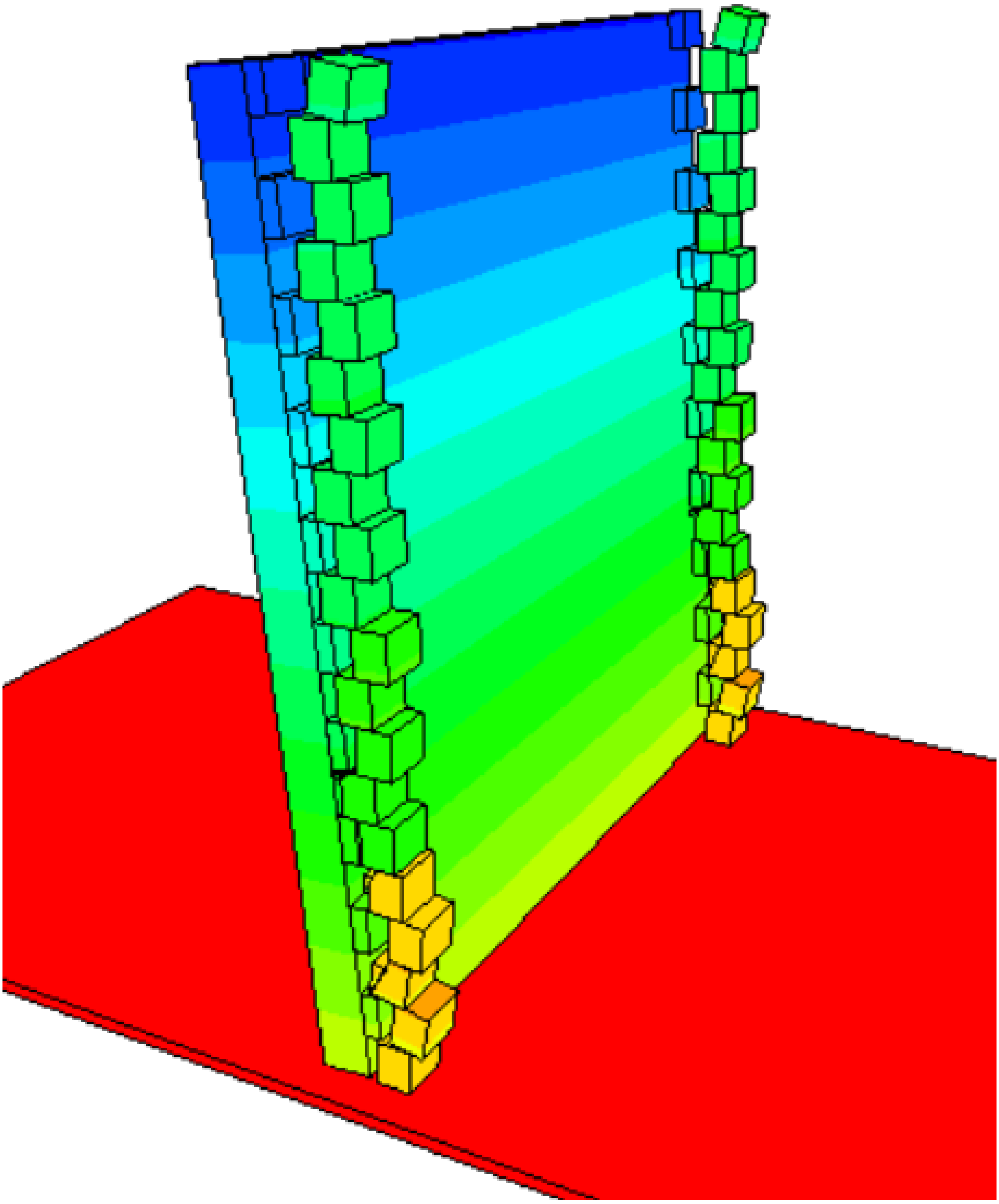

(c) W3

Figure 7: DEM modelling of rocking façade and return walls with associated block and spring interaction scheme (Colours represent displacement magnitude without scale).

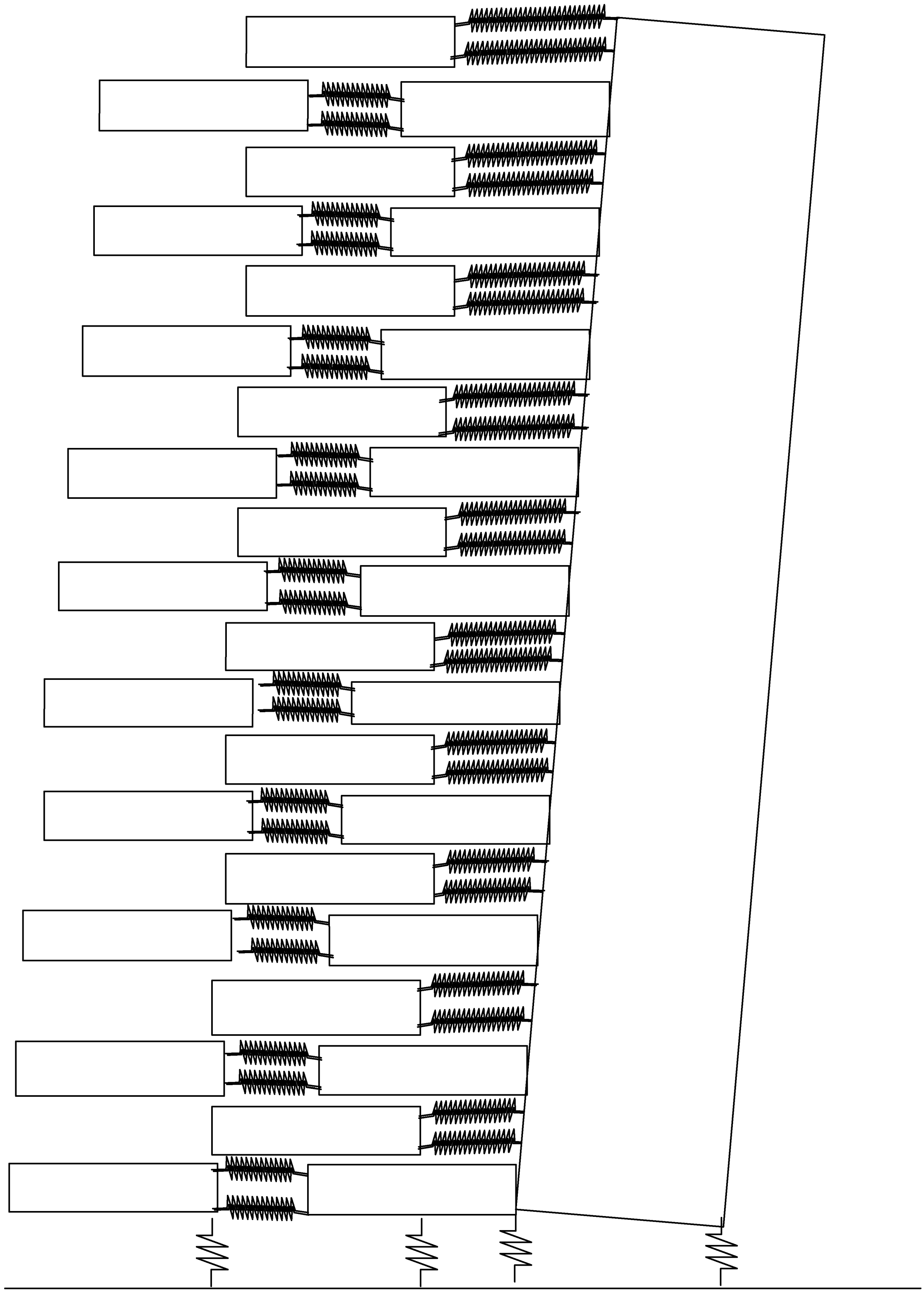

(c) W3

Figure 7: DEM modelling of rocking façade and return walls with associated block and spring interaction scheme (Colours represent displacement magnitude without scale).

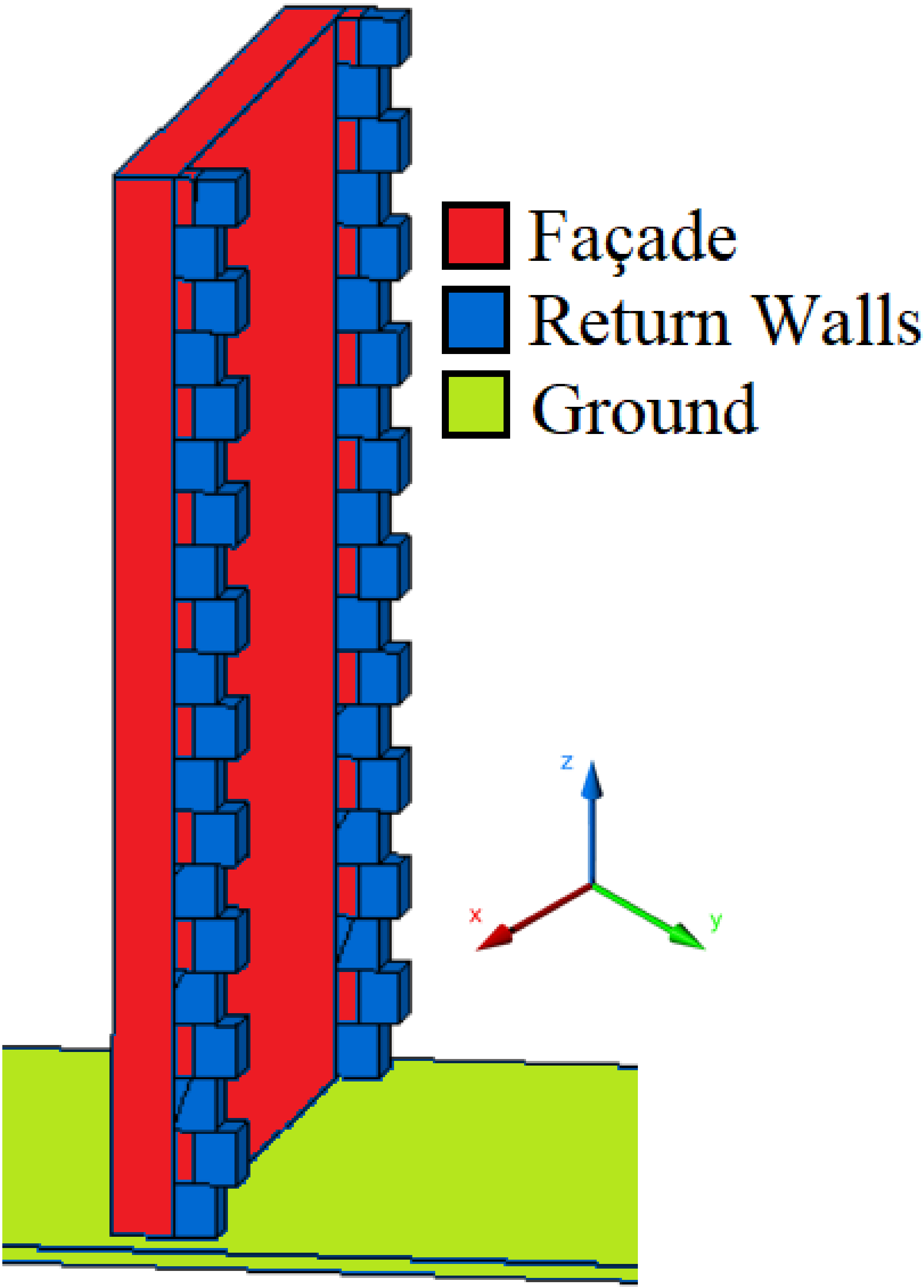

(a) Elements in W3

Figure 8: W3 details and capacity curve

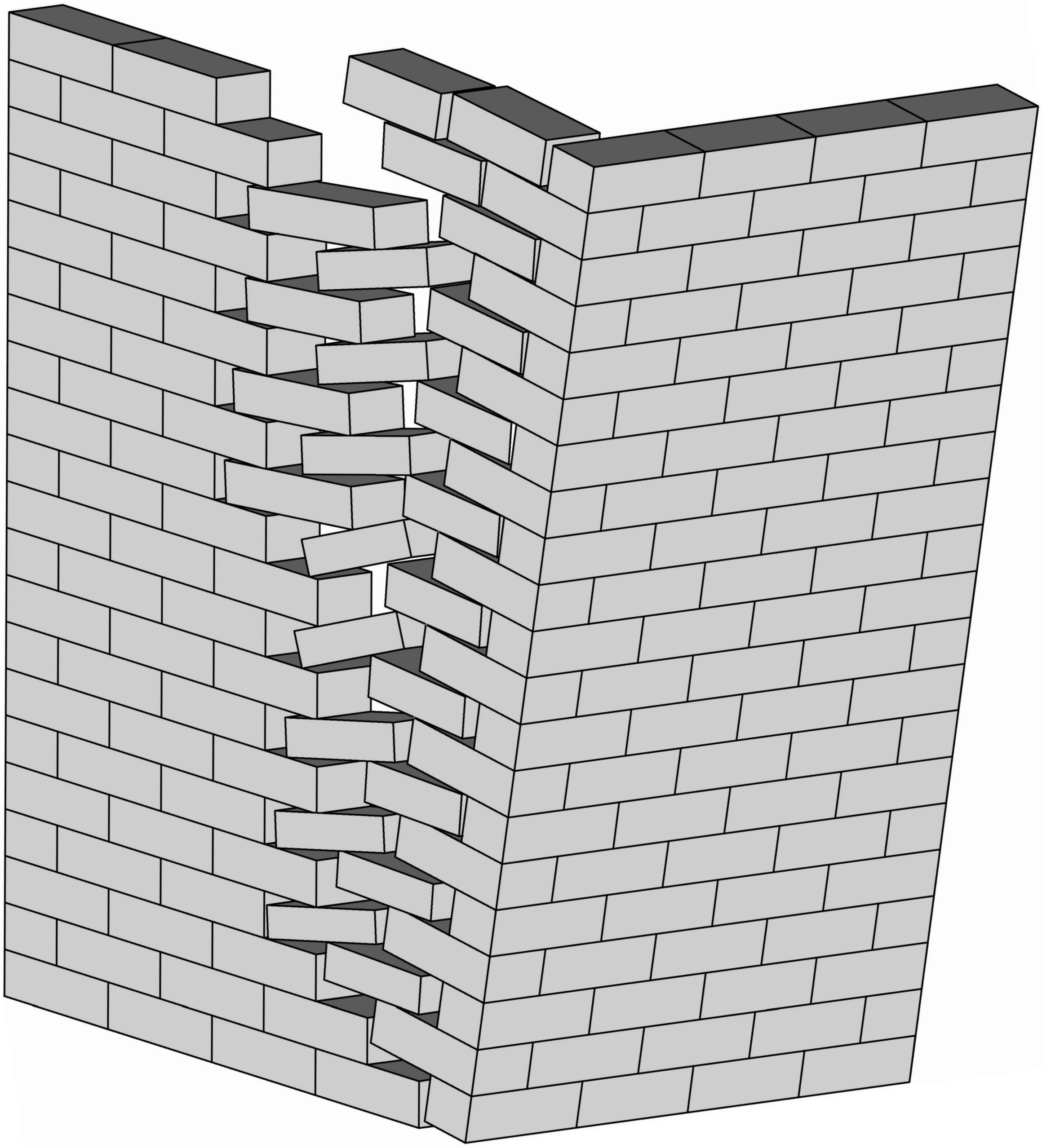

(b) Scheme of generic façade and return wall separation

Figure 8: W3 details and capacity curve

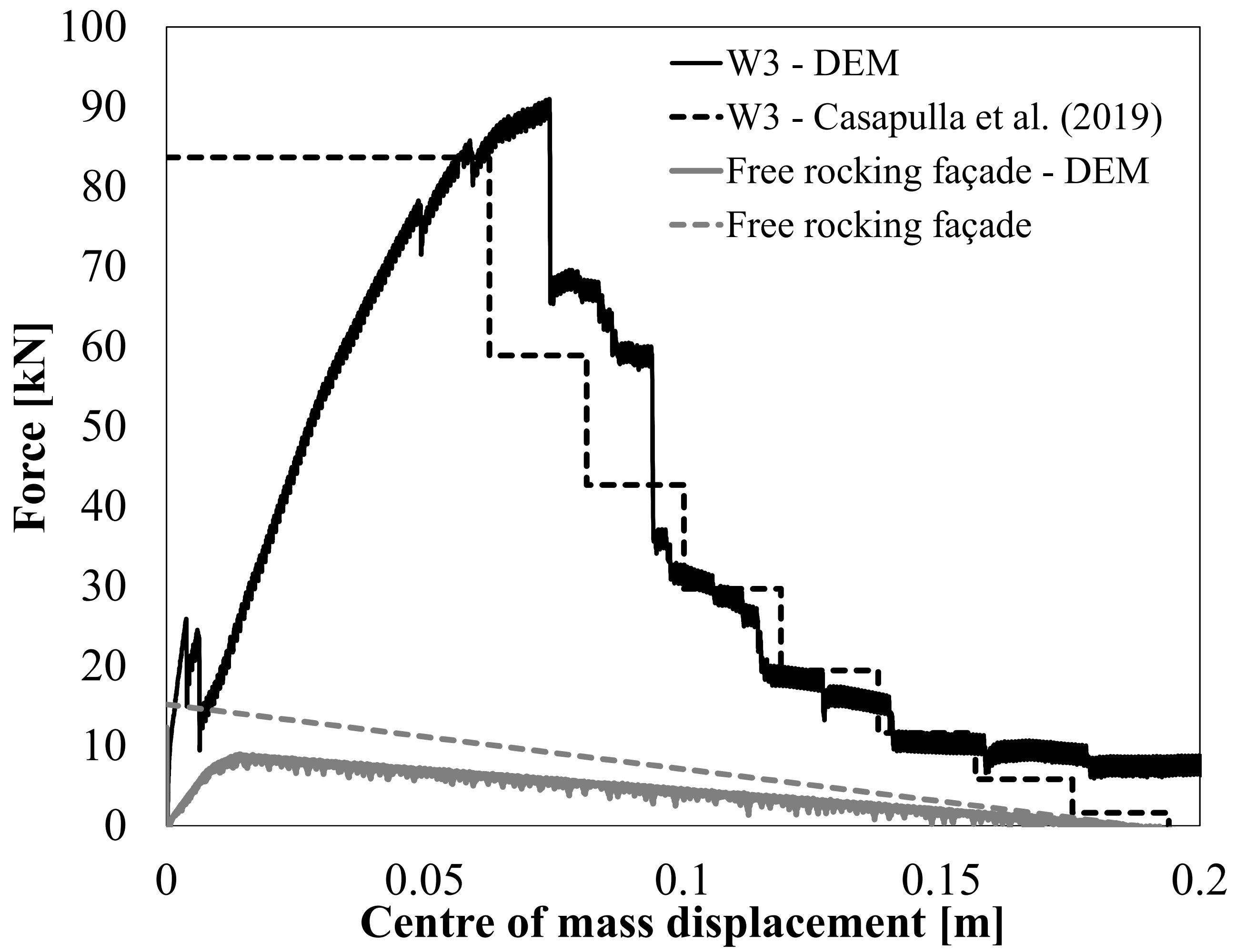

(c) Comparison between kinematic and DEM capacity curve

Figure 8: W3 details and capacity curve

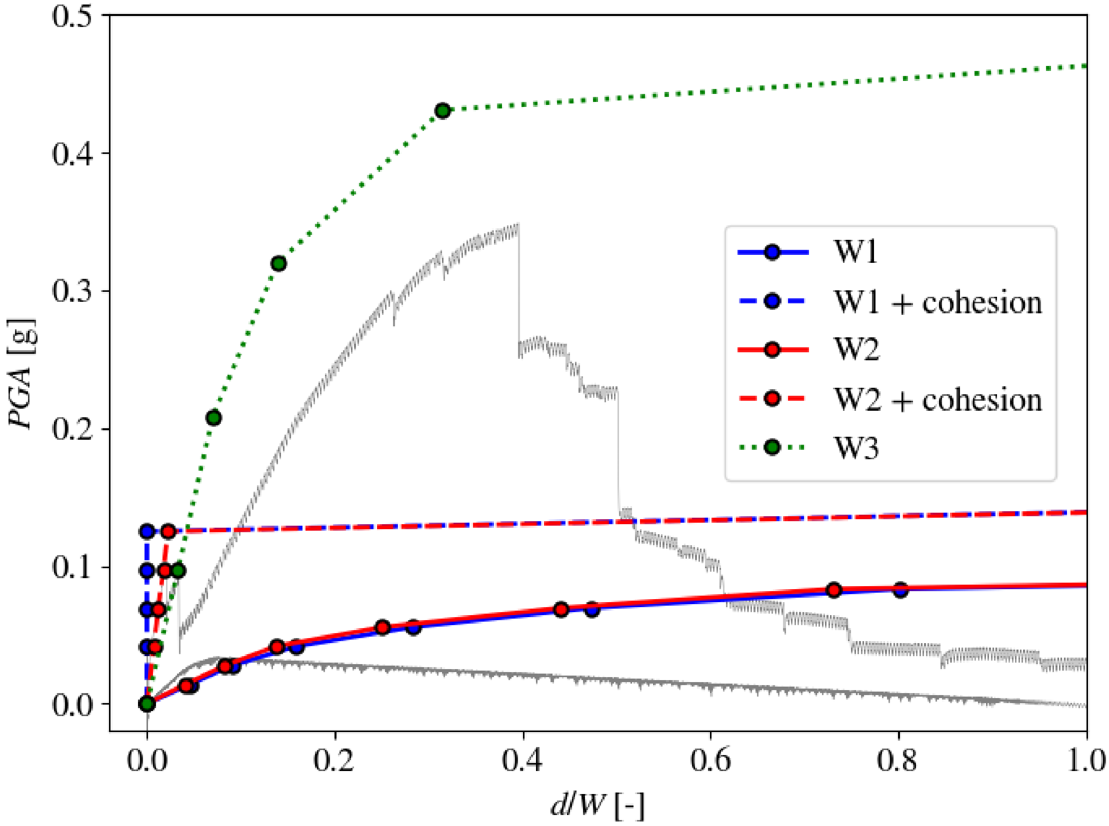

(a) BUCAR0 - Positive (+) direction

Figure 9: Incremental dynamic analyses. Pushover curves in grey for reference.

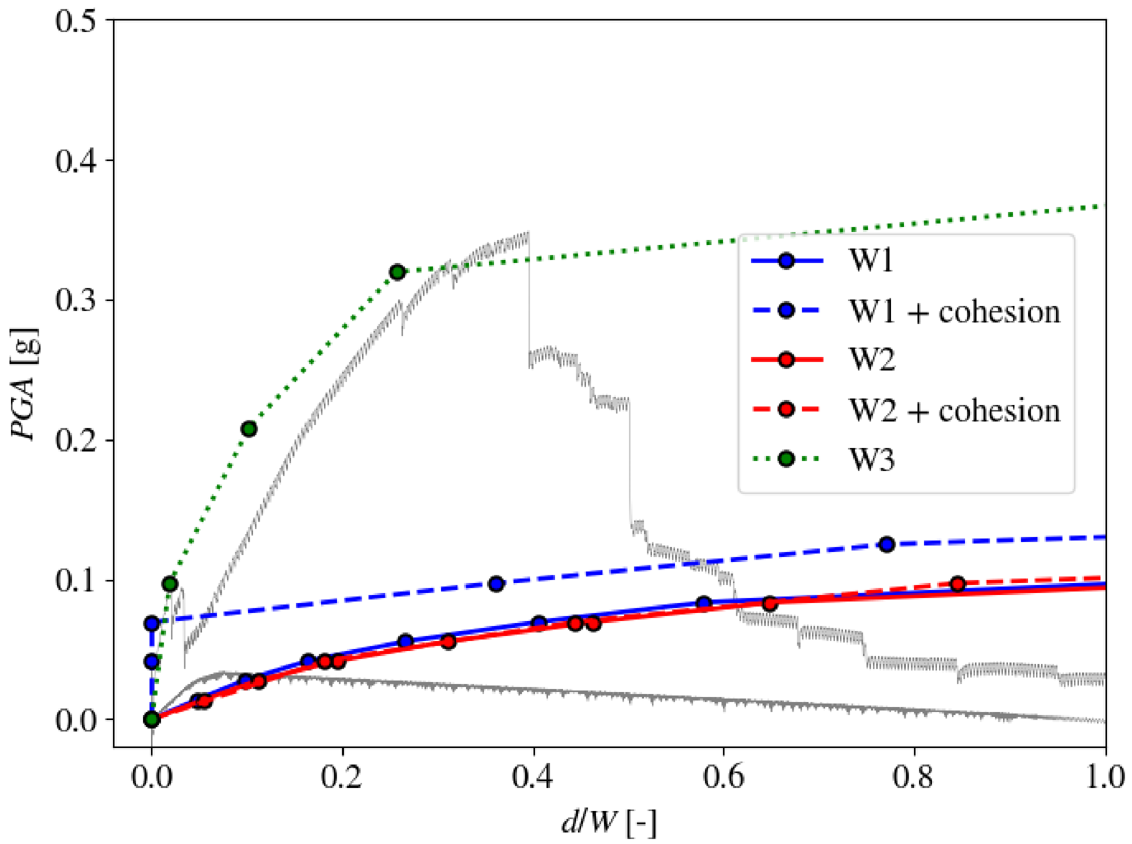

(a) BUCAR0 - Negative (-) direction

Figure 9: Incremental dynamic analyses. Pushover curves in grey for reference.

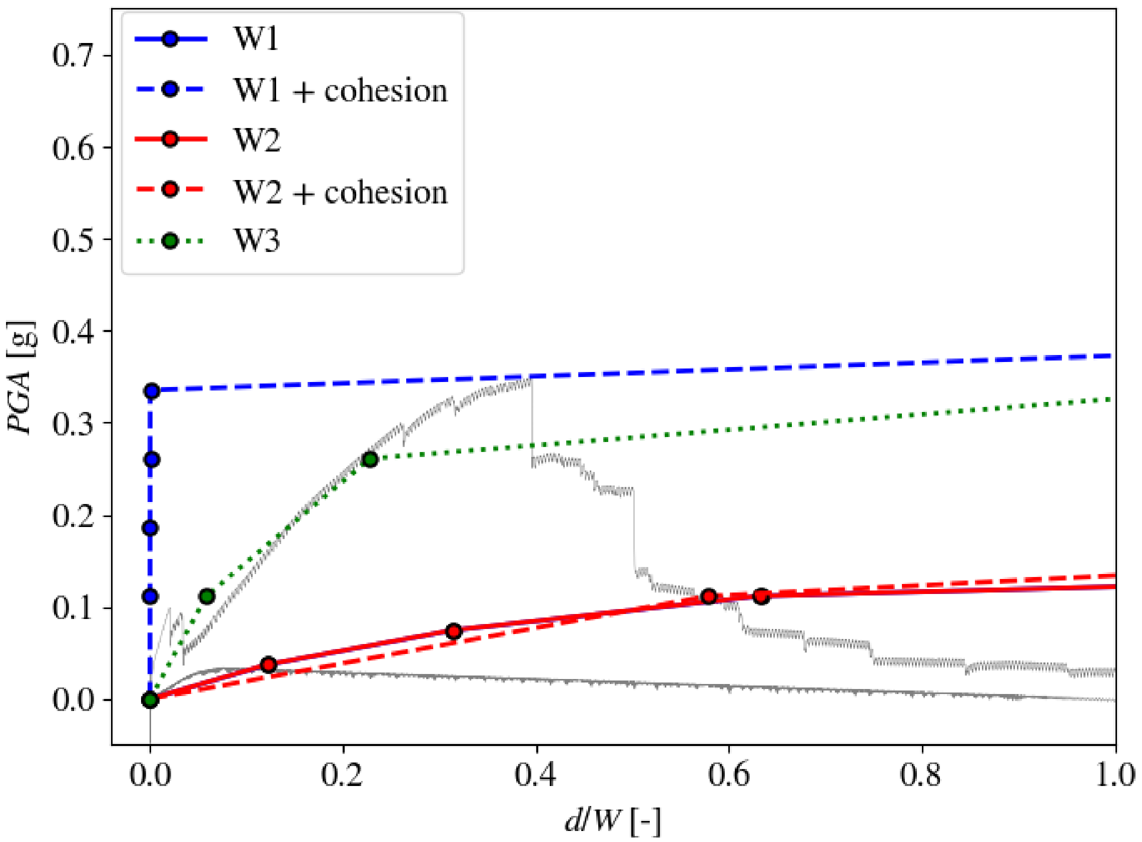

(b) RRS228 - Positive (+) direction

Figure 9: Incremental dynamic analyses. Pushover curves in grey for reference.

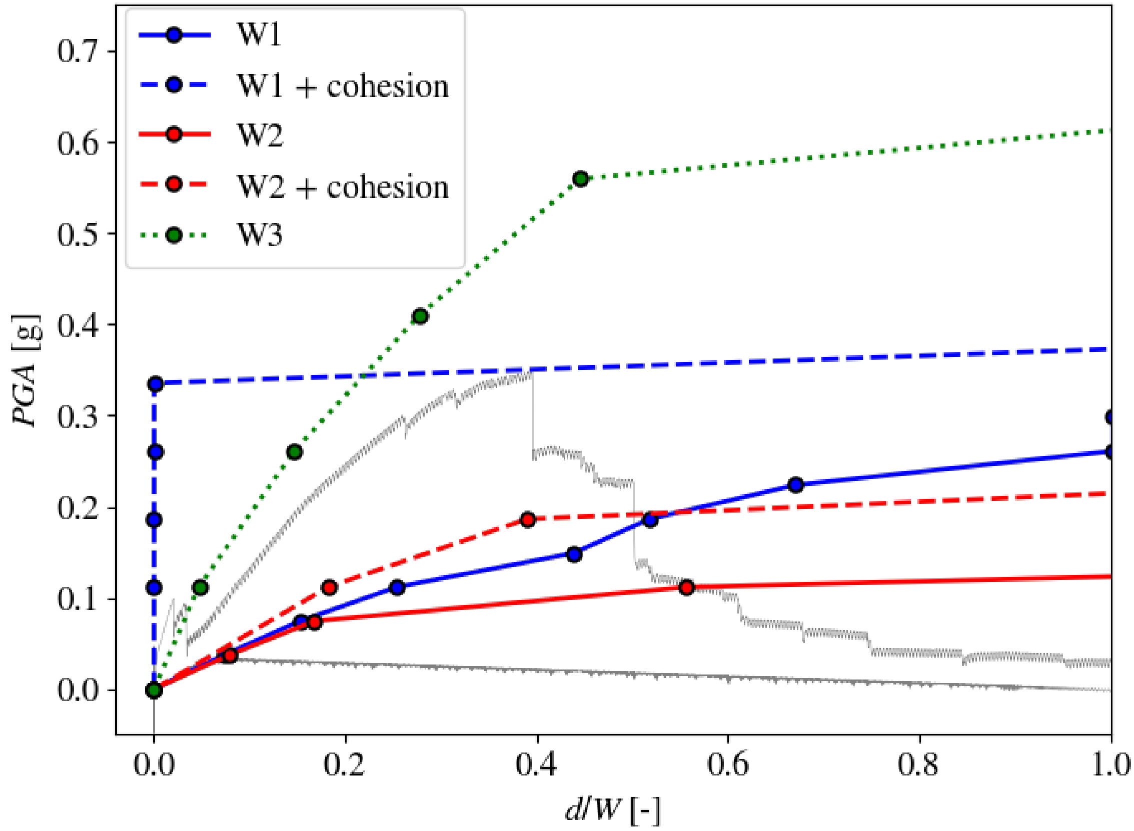

(b) RRS228 - Negative (-) direction

Figure 9: Incremental dynamic analyses. Pushover curves in grey for reference.

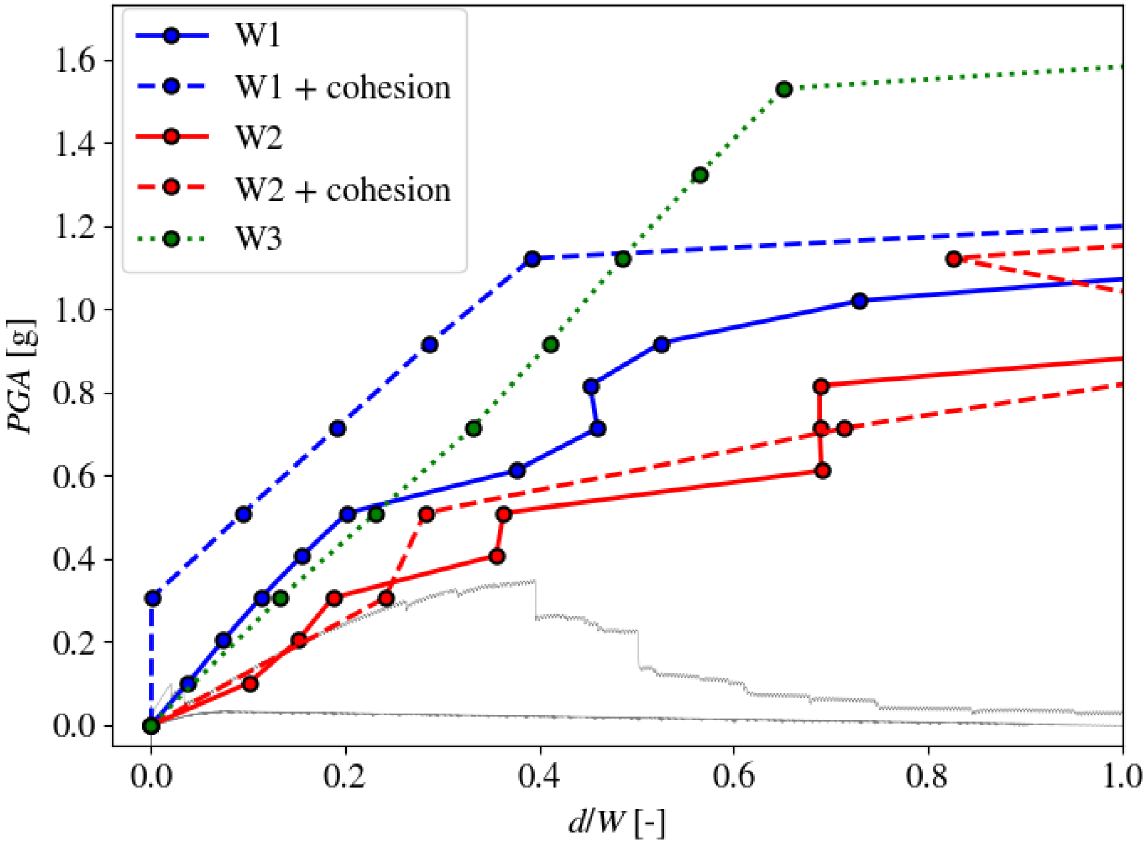

(c) 1ST280 - Positive (+) direction

Figure 9: Incremental dynamic analyses. Pushover curves in grey for reference.

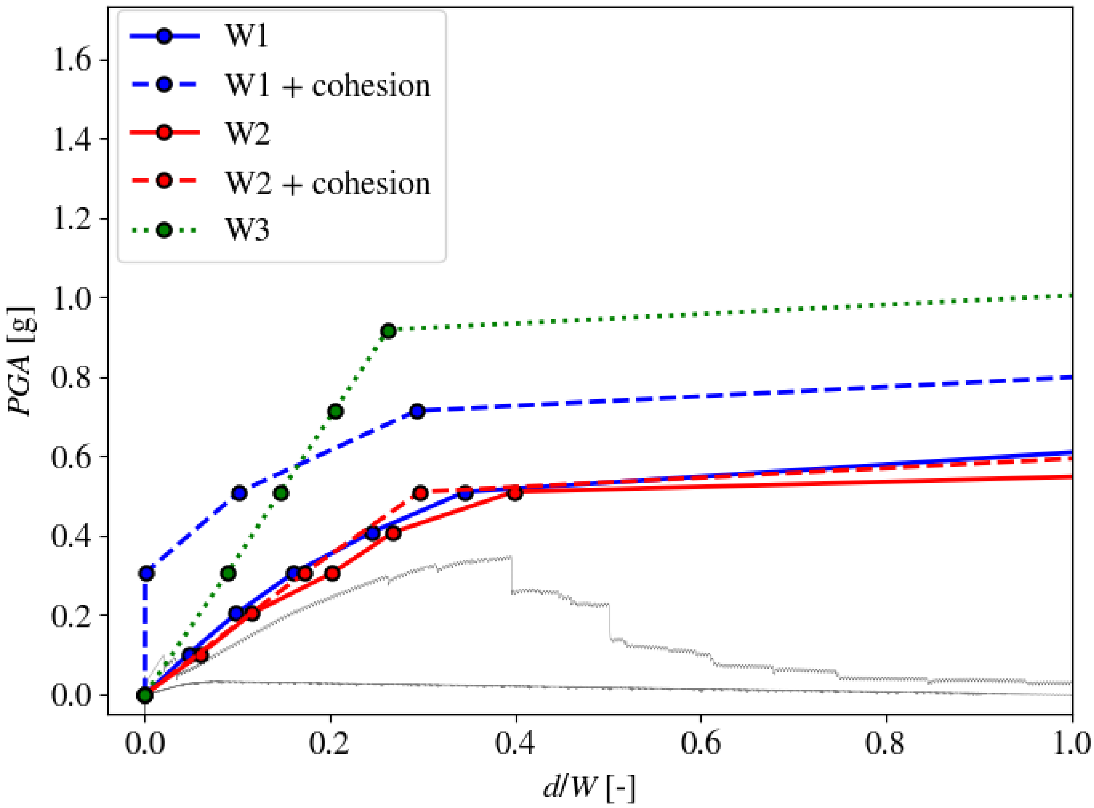

(c) 1ST280 - Negative (-) direction

Figure 9: Incremental dynamic analyses. Pushover curves in grey for reference.

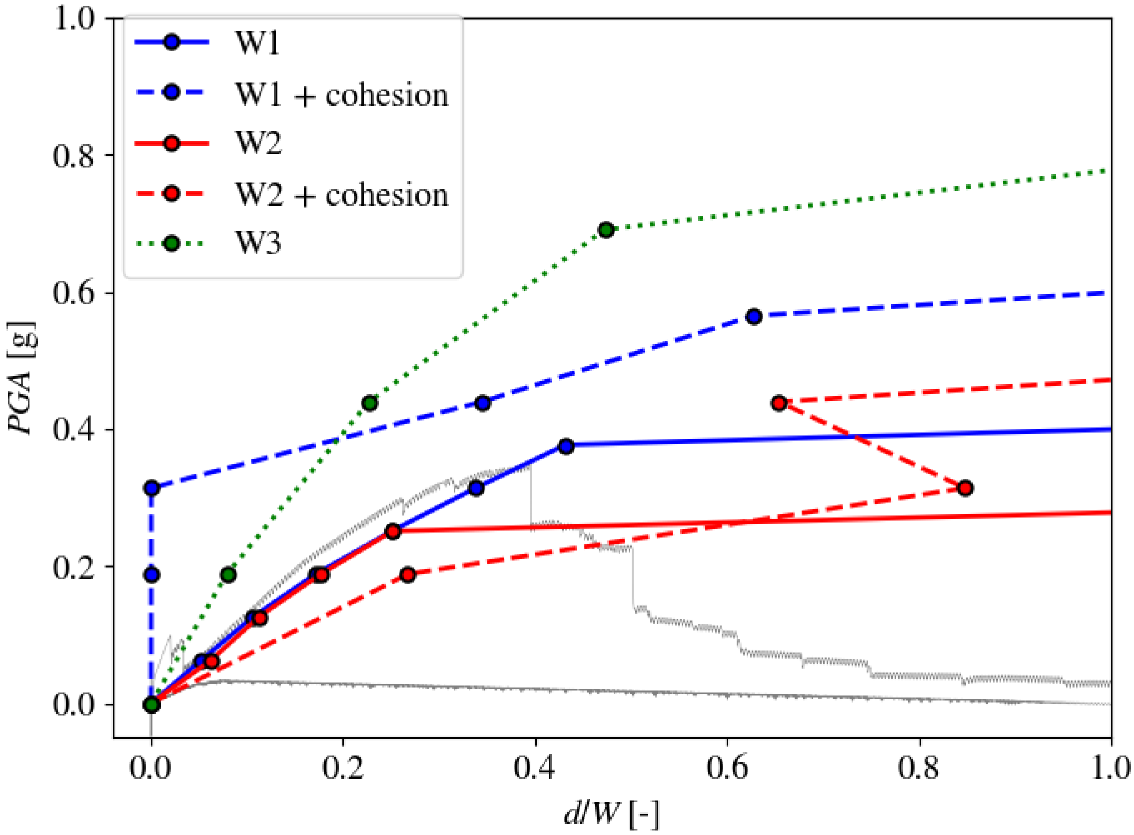

(d) HVSC1 - Positive (+) direction

Figure 9: Incremental dynamic analyses. Pushover curves in grey for reference.

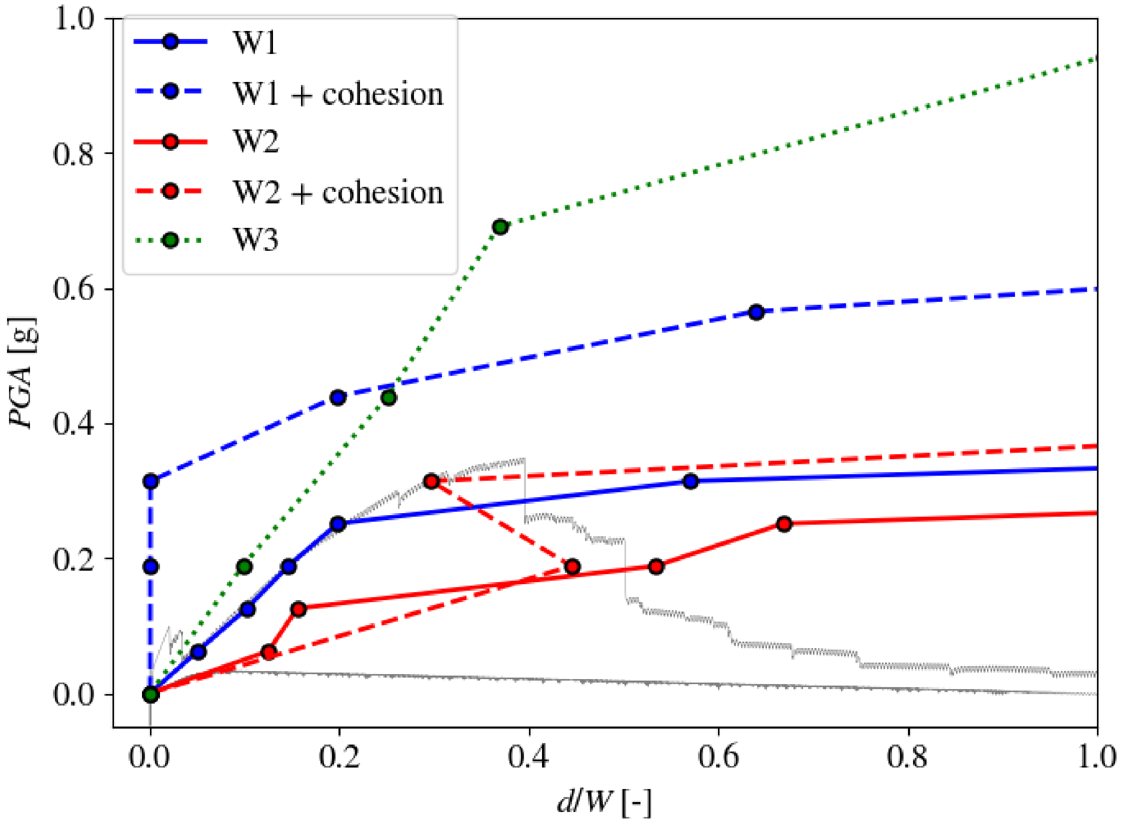

(d) HVSC1 - Negative (-) direction

Figure 9: Incremental dynamic analyses. Pushover curves in grey for reference.